Summer 2018

Lithospheric layering and thickness beneath the contiguous United States

Lin Liu

Department: Geosciences and Geological and Petroleum Engineering

LITHOSPHERIC LAYERING AND THICKNESS BENEATH THE CONTIGUOUS UNITED STATES

by

LIN LIU

A DISSERTATION

Presented to the Faculty of the Graduate School of the

MISSOURI UNIVERSITY OF SCIENCE AND TECHNOLOGY

In Partial Fulfillment of the Requirements for the Degree

DOCTOR OF PHILOSOPHY

in

GEOLOGY AND GEOPHYSICS

2018

Approved by:

Stephen Gao, Advisor

Kelly Liu, Co-Advisor

Wan Yang

Norbert Maerz

Jianguo Song

PUBLICATION DISSERTATION OPTION

This dissertation consists of the following two articles which have been published or submitted for publication as follows:

Paper I: Pages 3-33 have been published in the Journal of Geophysical Research: Solid Earth.

Paper II: Pages 34-76 have published in the Journal of the Earth Planetary Science Letter.

ABSTRACT

The Upper Mississippi Embayment (UME), where the seismically active New Madrid Seismic Zone resides, experienced two phases of subsidence commencing in the Late Precambrian and Cretaceous, respectively. To provide new constraints on models proposed for the mechanisms responsible for the subsidence, we computed and stacked P-to-S receiver functions recorded by 49 USArray and other seismic stations located in the UME and the adjacent Ozark Uplift and modeled Bouguer gravity anomaly data. The inferred thickness, density, and Vp/Vs of the upper and lower crustal layers suggest that the UME is characterized by a mafic and high-density upper crustal layer of ~30 km thickness, which is underlain by a higher-density lower crustal layer of up to ~15 km. Those measurements were the consequence of the passage of a previously proposed thermal plume. The thermoelastic effects of the plume would have induced wide-spread intrusion of mafic mantle material into the weak UME crust fractured by Precambrian rifting and increased its density, resulting in renewed subsidence after the thermal source was removed.

In addition, to image upper mantle seismic discontinuities beneath the contiguous United States, a total of 284,121 S-to-P receiver functions (SRFs) recorded by 3,594 broadband seismic stations in the EarthScope Transportable Array and other permanent and temporary deployments are stacked in circular bins of 2° in radius. A robust negative arrival, representing a sharp discontinuity of velocity reduction with depth, is visible in virtually all the stacked traces in the depth range of 30-110 km.

ACKNOWLEDGMENTS

First, I want to express my deepest and most profound appreciation to my advisors, Dr. Stephen Gao and Dr. Kelly Liu, for the continuous support of my Ph.D. study and related research, for their patient counsel and encouragement without reservation. From their tutelage, I have realized the meaning and requirement to be a scientist: pursuing the depths of truth, and 'no pains, no gains'. I could not have imagined having a better advisor and mentor for my Ph.D. study.

Besides my advisor, I would like to thank the rest of my dissertation committee members: Dr. Wan Yang, Dr. Norbert Maerz, and Dr. Jianguo Song, for their insightful comments and encouragement, but also for the questions which incented me to widen my research from various perspectives. Furthermore, I want to thank my friends and colleagues in the geophysics group of Missouri S&T, for the assistance, teamwork and all the fun we have had in the past five years.

Last but not least, I would like to thank my loving family. Words cannot express how grateful I am to my parents for all of the sacrifices that you have made on my behalf.

TABLE OF CONTENTS

Page

LIST OF ILLUSTRATIONS

Figure Page

PAPER I

PAPER II

LIST OF TABLES

NOMENCLATURE

Symbol	Description
PAPER I	
H	Candidate crustal thickness for station A
H_n	Candidate crustal thickness for station B
κ	Candidate Vp/Vs
Mc	cutoff magnitude
Δ	Epicentral distance in degree
D	Focal depth in kilometer
PAPER II	
p	S-wave ray parameter
h	Depth of the candidate discontinuity which ranges from 0 to 300 km with an interval of 1 km
Vp	P-wave velocity
Vs	S-wave velocity
β	Stretching factor

SECTION

1. INTRODUCTION

As demonstrated by numerous previous investigations, receiver functions using P-to-S and S-to-P converted waves at the discontinuities in the crust and upper mantle have been widely applied to measure the lithospheric layering and thickness. The Transportable Array (TA) component of the USArray project, which started in 2004 and has recently completed its coverage of the contiguous United States, has produced a broadband seismic data set at stations ∼70 km apart with unprecedented quality and spatial coverage, enabling the investigation of a wide spectrum of significant problems related to the structure and processes in the Earth's interior.

The dissertation is mainly composed of two parts. The first part delineates crustal thickness and Vp/Vs in the vicinity of the Upper Mississippi Embayment (UME) and the neighboring Ozark Uplift, two of the most significant geological features of the central United States. Although the crustal thicknesses of the United States have been measured by many previous P-to-S receiver function studies [Hansen et al., 2015; McGlannan and Gilbert, 2016; Shen and Ritzwoller, 2016], for some areas overlaying a loose Quaternary sedimentary layer, the strong reverberations mask the P-to-S phases from crust and mantle boundary, resulting in inaccurate measurements of crustal thicknesses and Vp/Vs ratios. This study estimates the crustal thickness, Vp/Vs, and density in the UME and adjacent areas through gravity modeling and H-κ stacking after removing the effects of the overlying sediments using a recently developed technique Yu et al. [2015a], for the purpose of constraining the subsidence models of the UME.

The second part measure the sub-crustal lithospheric layering beneath the contiguous United States based on S-to-P waves converted at the mid-lithospheric discontinuity (MLD) and lithosphere-asthenosphere boundary (LAB). The P-to-S phases from MLD/LAB are disturbed by crustal multiples because they arrive at similar time window and have similar amplitudes. In this study we image the depth of and S-to-P receiver function stacking amplitude associated with lithospheric discontinuities beneath the contiguous United States, with an unprecedented station coverage for the area. Additionally, we perform synthetic test on the possibility that the observed negative arrival corresponding to the negative-velocity discontinuity is an artifact from the Moho.

PAPER

I. RECEIVER FUNCTION AND GRAVITY CONSTRAINTS ON CRUSTAL STRUCTURE AND VERTICAL MOVEMENTS OF THE UPPER MISSISSIPPI EMBAYMENT AND OZARK UPLIFT

ABSTRACT

The Upper Mississippi Embayment (UME), where the seismically active New madrid seismic zone resides, experienced two phases of subsidence commencing in the Late Precambrian and Cretaceous, respectively. To provide new constraints on models proposed for the mechanisms of the subsidence, we computed and stacked P-to-S receiver functions recorded by 49 USArray and other seismic stations located in the UME and Ozark Uplift and modeled Bouguer gravity anomaly data. The thickness, density, and Vp/Vs of the upper and lower crustal layers suggest that the UME is characterized by a mafic and high-density upper crustal layer of ~30 km thickness, which is underlain by a higher-density lower crustal layer of up to ~15 km. Those measurements are in agreement with the model that the Cretaceous subsidence, which was suggested to be preceded by an approximately 2 km uplift, was the consequence of the passage of a previously proposed thermal plume. The thermoelastic effects of the plume would have induced wide-spread intrusion of mafic mantle material into the weak UME crust fractured by Precambrian rifting and increased its density, resulting in renewed subsidence after the thermal source was removed. In contrast, the Ozark Uplift has crustal density, thickness, and Vp/Vs measurements that are comparable to those observed on cratonic areas, suggesting an overall normal crust without significant modification by the proposed plume, probably owing to the relatively strong and thick lithosphere.

1. INTRODUCTION

The Transportable Array (TA) component of the USArray project, which started in 2004 and has recently completed its coverage of the contiguous United States, has produced a broadband seismic data set at stations ~70 km apart with unprecedented quality and spatial coverage, enabling the investigation of a wide spectrum of significant problems related to the structure and processes in the Earth's interior. This study takes advantage of the outstanding data set from the TA and other networks and employs a recently developed modified version of a widely used technique for crustal studies, the H-κ (or thickness-Vp/Vs) stacking [Zhu and Kanamori, 2000; Yu et al., 2015a], to delineate crustal thickness and Vp/Vs in the vicinity of the Upper Mississippi Embayment (UME) and the neighboring Ozark Uplift, two of the most significant geological features of the central United States.

1.1. TECTONIC SETTING

The UME (Figure 1), where the seismically active New Madrid Seismic Zone (NMSZ) resides, is a broad southwest plunging trough with a complex rifting, uplift, and subsidence history in the heart of the relatively stable North American continent [Mooney et al., 1983; Thomas, 1991; Catchings, 1999; Van Arsdale and Cox, 2007]. The center of the UME is occupied by the Reelfoot Rift formed within the Precambrian Eastern Granite-Rhyolite Province (1470 ± 30 Ma) and Southern Granite-Rhyolite Province (1370 ± 30 Ma) [VanSchmus, 1992]. Thegranite provinces are also home to the Ozark Uplift, a 150,000 km2 intracratonic highland region located to the west of the Reelfoot

Rift and eroded to expose Precambrian granites and rhyolites [Van Schmus, 1992; Liang and Langston, 2009].

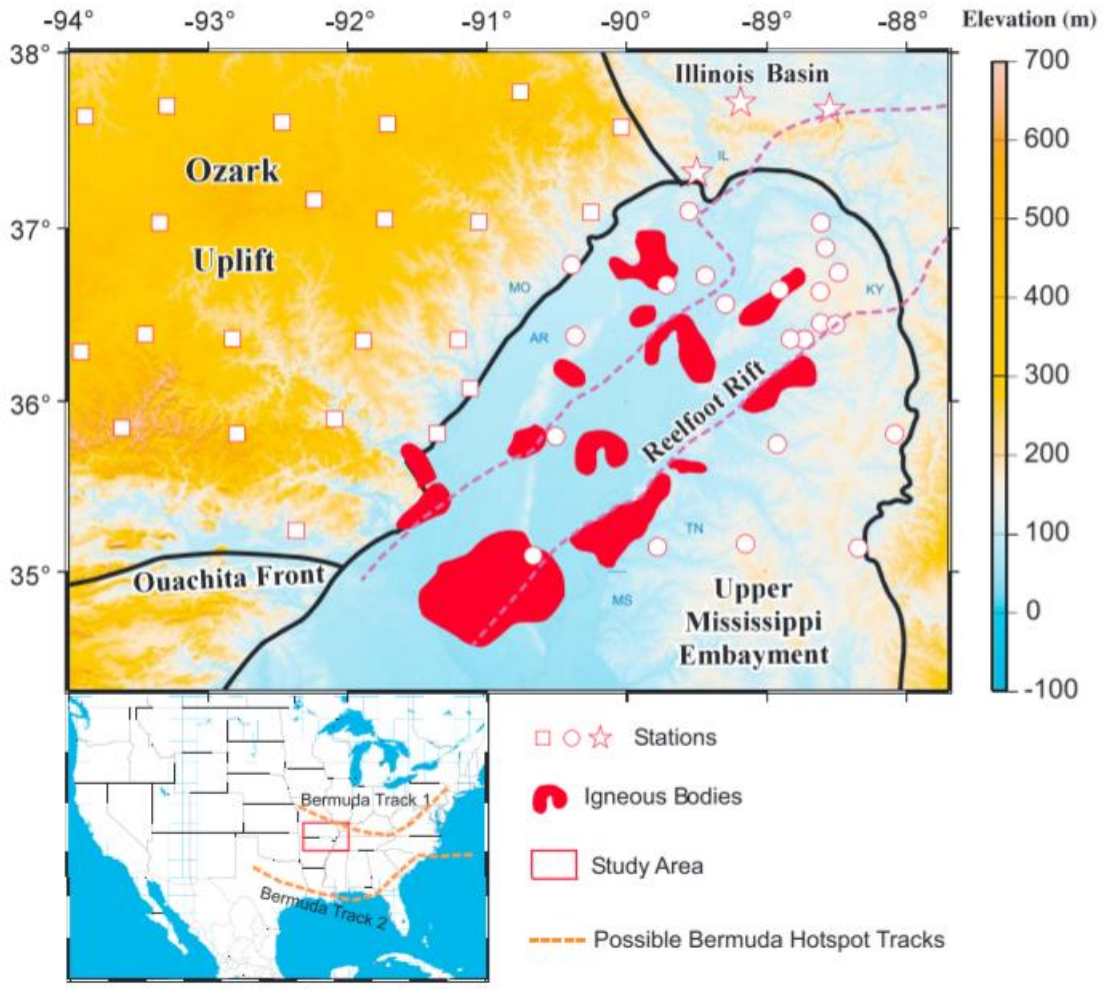

Figure 1. Topographic map showing boundaries of major tectonic features (black lines), igneous bodies (red areas) [Hildenbrand et al., 1996], and broadband seismic stations used in the study. Stations represented by squares, circles, and stars are located in the Ozark Uplift, Upper Mississippi Embayment, and the Illinois Basin, respectively. The area between the purple dashed lines is the Reelfoot Rift, in which the NMSZ is located. The inset in the lower left corner displays the map of the contiguous United States showing the location of study area (red rectangle) and proposed possible Bermuda hotspot tracks (orange dash lines) [Pollitz and Mooney, 2014].

Unlike many other continental rifts which have a single phase of subsidence [e.g., Logatchev and Florensov, 1978; Keller et al., 1991], the Reelfoot Rift experienced two distinct phases of subsidence separated by about 250 Ma of relative tectonic quiescence [Ervin and McGinnis, 1975]. The initial rifting phase began during the Late Precambrian, when the North American Plate experienced wide-spread rifting events [Ervin and McGinnis, 1975]. The major basinal development period was in the Cambrian-Ordovician time, as determined by drilling [Schwalb, 1969; Ervin and McGinnis, 1975]. The second phase of subsidence, which was responsible for the accumulation of several kilometers of deltaic and marine sediments and was coeval with the emplacement of mafic igneous intrusions found inside and along the shoulders of the rift (Figure 1), started in the Cretaceous and may have continued until the present time and is believed to be the ultimate cause of the high seismicity level in the NMSZ [Mooney et al., 1983; Hildenbrand and Hendricks, 1995; Cox and Van Arsdale, 2002].

Several models have been proposed for the second (or reactivation) phase of subsidence. The first model attributes the renewed subsidence of the UME to the extensional stress regime associated with the opening of the Gulf of Mexico [Ervin and McGinnis, 1975; Kane et al., 1981]. However, this model has been questioned because the subsidence did not start until about 80 Ma after the cessation of the rifting of the Gulf margin [Cox and Van Arsdale, 1997]. The second model postulates that the later phase of subsidence of the UME represents isostatic adjustment of a high-density, mafic lower crustal layer during a period of decreased lithospheric viscosity owing to increased geothermal gradient [DeRito et al., 1983; Braile et al., 1986]. The third model advocates the role that the proposed Bermuda mantle plume played during its passage over the

previously rifted area [Cox and Van Arsdale, 1997], leading to uplift, intrusion of high-density igneous rocks into the crust, erosion of the uplifted axial area of the UME, and subsidence due to thermal contraction and loading of both the sediments and dense intrusions [Cox and Van Arsdale, 1997].

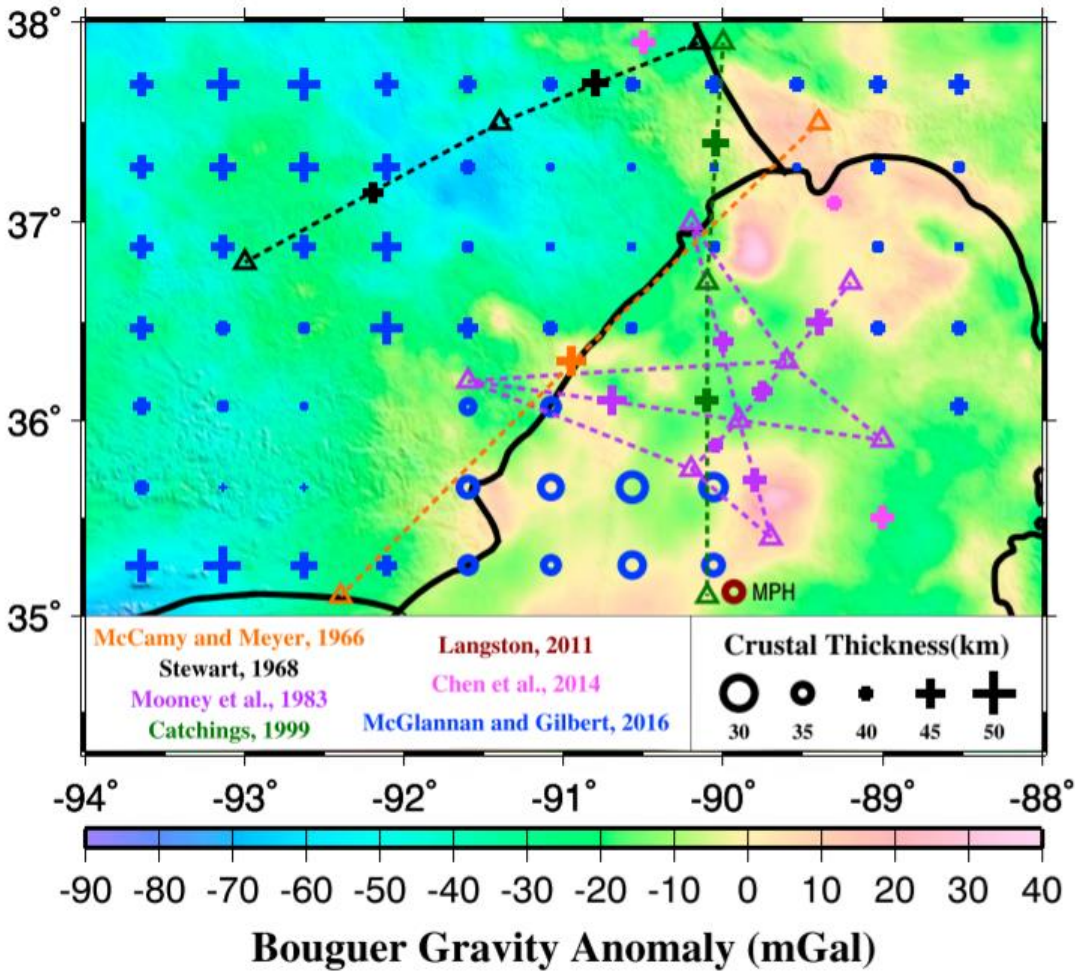

Figure 2. Previous determinations of crustal thickness plotted on top of Bouguer gravity anomalies. Pluses and circles indicate larger and smaller H measurements, respectively (see legend). Dashed lines indicate seismic refraction profiles, and triangles are shot points [McCamy and Meyer, 1966; Stewart, 1968; Mooney et al., 1983; Catchings, 1999].

This study aims at providing constraints on the proposed subsidence models by measuring crustal thickness and the bulk composition beneath the UME and the adjacent Ozark Uplift. It represents the first joint receiver function (RF) and gravity data investigation of the crustal thickness, Vp/Vs, and density for the study area.

1.2. PREVIOUS CRUSTAL STRUCTURE INVESTIGATIONS

Numerous geophysical studies have been conducted in the vicinity of the UME over the past decades for the purpose of understanding the formation mechanism of active faults associated with the intracontinental earthquakes occurring in the area. The most significant results regarding crustal thickness, P wave velocity, and layered structures were from active-source seismic refraction/wide-angle reflection surveys [McCamy and Meyer, 1966; Mooney et al., 1983; Catchings, 1999]. One of the major discoveries reported by virtually all the active-source studies is that the lowest 10–20 km of the crust beneath the UME has a Vp of about 7.3–7.4 km/s which is about 10% higher than that of a typical continental lower crust. This lower crustal layer is directly above the Moho, which has a depth of 43–46 km in the UME [McCamy and Meyer, 1966; Mooney et al., 1983; Catchings, 1999].

Due to the limited spatial coverage of the active source seismic profiles as a result of the high cost of such experiments, the lateral extent of this layer is not well defined beneath the UME, and the Ozark Uplift was poorly sampled by the above profiles (Figure 2). In addition, because only P wave velocities are measured, the Vp/Vs, which is closely related to rock composition and physical properties [Christensen and Mooney, 1995], is not available at most of the areas with the exception of a N-S profile of about 400 km

length across the UME (Figure 2) [Catchings, 1999]. Vp/Vs values were estimated along the profile in several crustal layers, but because the shear wave arrivals cannot be clearly picked, the results suffer from large uncertainties [Catchings, 1999].

Source-normalized P-to-S converted phases from the Moho, i.e., RFs [Langston, 1977], have been routinely used to measure crustal thickness (H) and most recently Vp/Vs [Zhu and Kanamori, 2000] over a large area with relatively low cost. A recent RF study that is most relevant to the present one was conducted by McGlannan and Gilbert [2016]. Using RFs recorded by the USArray TA stations, the study concludes that the depth of the Moho beneath the UME is mostly 30–35 km, which is shallower than that of the surrounding areas (40–45 km) and is also shallower than the ~45 km depth reported by most of the active-source seismic studies. Instead of simultaneously searching for both the optimal H and Vp/Vs [Zhu and Kanamori, 2000], a fixed Vp/Vs of 1.785 was used for the stacking in the McGlannan and Gilbert [2016] study, and the results were obtained for overlapping 0.5∘ by 0.5∘ bins (rather than at the stations; Figure 2). As demonstrated by the examples shown in Figure 3, RFs in the UME may have been contaminated by strong reverberations generated in the loose sedimentary layer covering most of the UME, and thus, studies using raw RFs might have produced biased results.

1.3. RATIONALE OF THE PRESENT STUDY

Although many previous studies have estimated the crustal thickness beneath the NMSZ and adjacent areas, the active-source seismic experiments were limited to 2-D profiles that traversed only part of the UME (Figure 2) and thus have a limited spatial coverage, making it difficult to compare results from various portions of the UME and

with the surrounding areas. More importantly, the calculation of the Vp/Vs, which is crucial for the understanding of tectonic processes that have modified the crust, has yet to be performed on the majority of the stations. The lack of reliable Vp/Vs determinations is most likely caused by the strong reverberations on the RFs associated with the loose sedimentary layer. This study estimates the crustal thickness, Vp/Vs, and density in the UME and adjacent areas through gravity modeling and H-κ stacking after removing the effects of the overlying sediments using a recently developed technique Yu et al. [2015a], for the purpose of constraining the subsidence models of the UME.

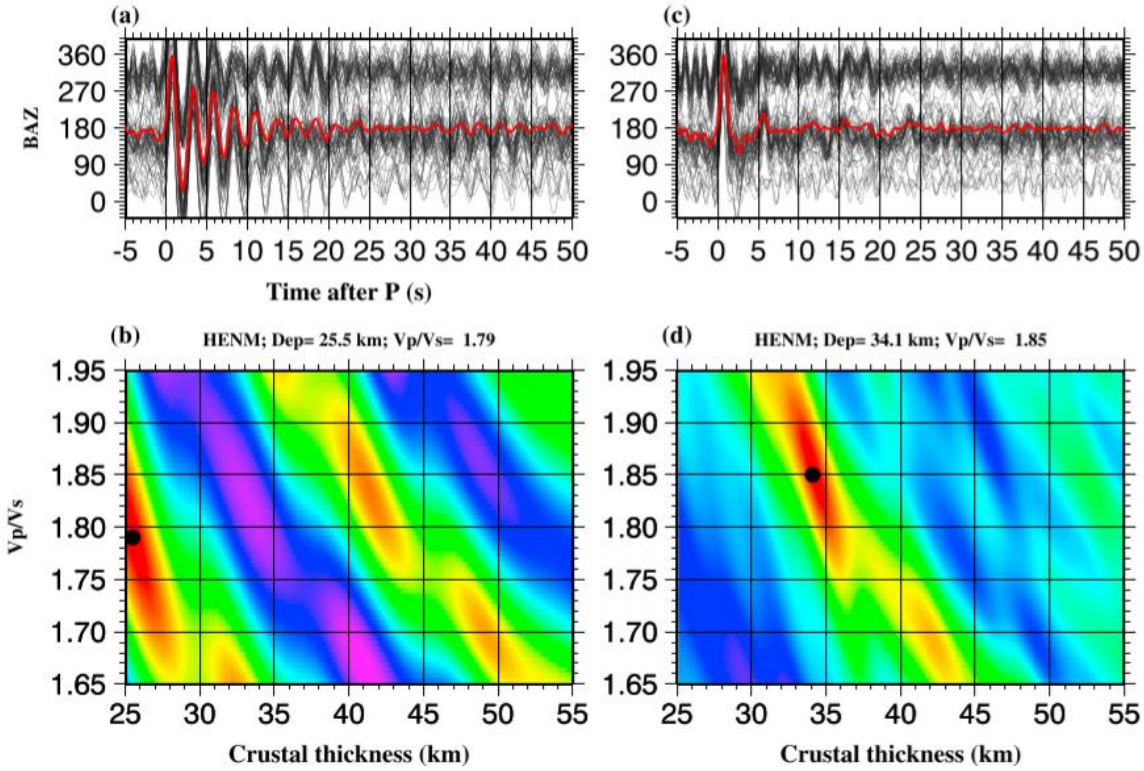

Figure 3. (a) Original RFs from station HENM plotted against back azimuth (BAZ). The red trace is the result of simple time domain summation of the individual RFs and demonstrates the strong decaying periodic arrivals of the reverberations. (b) H-κ stacking using the raw RFs shown in Figure 3a. The dot denotes the maximum stacking amplitude. (c) Same as Figure 3a but for RFs after removing the reverberations using the approach of Yu et al. [2015a]. (d) H-κ stacking using the filtered RFs shown in Figure 3c.

Table 1. Observations of Crustal Thickness (H, H_n) and Vp/Vs (κ)

Stn	Lon.	Lat.	H(km)	ϕ	H_n(km)	N	Rank
			Ozark Uplift				
HHAR	-93.940	36.282	41.1± 0.06	1.800± 0.000	–	314	A
LCAR	-91.154	36.070	42.1± 0.07	1.790± 0.000	–	329	A
MGMO	-92.269	37.154	45.9± 0.19	1.823± 0.005	–	426	A
S38A	-93.908	37.630	40.6± 0.14	1.780± 0.009	–	126	A
S39A	-93.323	37.691	44.5± 0.14	1.830± 0.000	–	221	A
S40A	-92.501	37.599	47.2± 0.11	1.754± 0.005	–	140	A
S41A	-91.746	37.588	–	–	43.9± 0.05	139	B
S42A	-90.794	37.770	42.1± 0.34	1.797± 0.013	–	99	A
S43A	-90.075	37.572	–	–	41.6± 0.06	115	B
T39A	-93.377	37.024	44.2± 0.15	1.798± 0.004	–	143	A
T41A	-91.764	37.044	43.0± 0.19	1.764± 0.005	–	115	A
T42A	-91.092	37.030	–	–	39.1± 0.33	151	B
T43A	-90.288	37.083	39.7± 0.28	1.771± 0.007	–	105	A
U39A	-93.480	36.382	41.1± 0.17	1.818± 0.004	–	149	A
U40A	-92.854	36.356	39.7± 0.15	1.819± 0.003	–	333	A
U41A	-91.920	36.344	–	–	44.3± 0.23	136	B
U42A	-91.238	36.351	–	–	42.9± 0.20	104	B
V39A	-93.645	35.839	–	–	45.2± 0.08	151	B
V40A	-92.823	35.804	40.5± 0.03	1.800± 0.000	–	136	A
V41A	-92.124	35.890	37.6± 0.14	1.806± 0.005	–	459	A
V42A	-91.390	35.806	38.8± 0.16	1.770± 0.005	–	101	A
X301*	-92.400	35.239	50.3± 0.39	1.838± 0.004	–	53	A
			Upper Mississippi Embayment				
CUSSO*	-89.330	36.552	29.6± 0.28	1.879± 0.017	–	24	A
DHKY*	-88.941	36.635	30.7± 0.95	1.869± 0.026	–	14	A
HENM*	-89.472	36.716	34.0± 0.14	1.853± 0.007	–	95	A
JLKY*	-88.652	36.624	34.4± 0.67	1.888± 0.028	–	35	A
JRTN*	-88.648	36.443	33.3± 0.33	1.857± 0.013	–	53	A
MMTN*	-88.539	36.434	–	–	32.7± 0.37	28	B
NKKY*	-88.520	36.734	–	–	34.5± 0.20	34	B
PARM*	-89.752	36.664	37.7± 0.22	1.788± 0.008	–	104	A
PBMO	-90.430	36.778	40.0± 0.14	1.830± 0.000	–	545	A
RPTN*	-88.763	36.348	32.5± 0.35	1.859± 0.022	–	29	A
S01*	-89.539	36.314	33.6± 0.51	1.913± 0.016	–	110	A
T44A	-89.590	37.086	–	–	38.6± 0.57	103	B
T45A*	-88.645	37.020	38.3± 0.26	1.867± 0.005	–	103	A
U43A*	-90.406	36.369	36.0± 0.73	1.883± 0.016	–	92	A
U45A*	-88.763	36.348	32.9± 0.24	1.840± 0.006	–	40	A
UTMT*	-88.864	36.350	31.9± 0.27	1.927± 0.010	–	263	A
V43A*	-90.544	35.786	–	–	26.8± 0.16	20	B
V45A*	-88.959	35.740	30.4± 0.00	1.843± 0.005	–	72	A
V46A	-88.118	35.801	–	–	33.9± 0.07	76	B
W43A*	-90.706	35.088	31.0± 0.35	1.864± 0.019	–	16	A
W44A*	-89.816	35.139	–	–	33.5± 0.18	44	B
W45A*	-89.186	35.157	–	–	32.7± 0.13	124	B
W46A	-88.378	35.133	–	–	37.5± 0.23	84	B
WBKY*	-88.613	36.877	–	–	37.5± 0.09	38	B
			Illinois Basin				
FA08	-89.529	37.316	42.0± 0.48	1.808± 0.018	–	75	A
S44A*	-89.217	37.715	44.2± 1.11	1.783± 0.019	–	1215	A
S45A*	-88.580	37.677	–	–	45.9± 0.73	146	B

∗ After applying the reverberation-removal technique.

2. DATA AND METHODS

All the three-component broadband teleseismic (epicentral distance ≥30°) data were obtained from the Incorporated Research Institutions for Seismology (IRIS) Data Management Center (DMC) within the area of 94°W–88°W and 34°N–38°N (Figure 1) for the time frame from September 1989 to April 2015, when the USArray TA stations completed their recording in the area. A cutoff magnitude (Mc), which is calculated using Mc =5.2+ (Δ −30.0)/(180.0−30.0) –D/700.0, where Δ and D are the epicentral distance in degree and focal depth in kilometers, respectively, is used to select earthquakes [Liu and Gao, 2010].

The seismograms were windowed starting 20 s prior to and extending to 260 s after the first theoretical P wave arrival according to the IASP91 Earth model [Kennett and Engdahl, 1991]. After being band pass filtered within the frequency range of 0.04 to 1.0 Hz, all the events having a P wave signal-to-noise ratio of 4.0 or greater on the radial component were selected and converted into radial RFs using the water level deconvolution procedure described in Ammon [1991], with a water level of 0.03 and a Gaussian filter width of 5.0. Subsequently, the radial RFs were inspected visually to keep only the ones with a well-defined first arrival in the 0-2 second window. A total of 7627 high-quality RFs are used in the study.

Strong reverberations in the resulting RFs produced by multiple reflections between the Earth's surface and the bottom of a loose sedimentary layer can seriously mask the P-to-S converted phases (PmS, PPmS, and PSmS) from the Moho (Figure 3), leading to erroneous crustal thickness and Vp/Vs determinations beneath a recording site

[Zelt and Ellis, 1999; Yu et al., 2015a]. A resonance-removal filter in the frequency domain is designed to remove or significantly reduce the reverberations [Yu et al., 2015a]. After removing the travel times associated with the loose sedimentary layer, the conventional H-κ stacking method [Zhu and Kanamori, 2000] can then be employed to determine the crustal thickness and Vp/Vs (Figure 3) beneath the loose sedimentary layer, which is less than 1 km thick in the study area [Dart and Swolfs, 1998]. Among the 49 stations that led to reliable H results, 23 were processed with the reverberation removal technique (Table 1). Figure 4 shows examples of the H-κ diagram, and Figures S1–S4 in the supporting information show all the H-κ diagrams and the RFs used to produce them.

An accurate average crustal P wave velocity is essential to produce reliable results from the H-κ stacking. Previously estimated average crustal Vp beneath the UME ranges from 6.0 to 6.4 km/s [Mooney et al., 1983; Chiu et al., 1992; Catchings, 1999; Ramírez-Guzmán et al., 2012]. After considering results from various studies and also the presence of both the low-velocity sedimentary layer and high-velocity lower crust, in this study, we use an average P wave velocity of 6.1 km/s, which is the same as that in the IASP91 Earth model. Nair et al. [2006] stack 66 CORE (Complete Ordered Ray Expansion) synthetic seismograms to estimate the magnitude of error when an inaccurate Vp is used. They show that if the velocity has a 1% bias, the resulting crustal thickness will be off by about 0.5 km. Likewise, the resulting Vp/Vs will vary by 0.0024 with a 1% bias in Vp. In the study area, previous studies show that the mean crustal velocity is unlikely to depart from 6.1 km/s by more than Figure 4. Image of stacking energy from H-κ stacking using the filtered RFs from stations JRTN and U45A located in the UME. The black dots and

triangles show points with the first and second largest stacking amplitudes, corresponding to the top and bottom of a lower crustal layer, respectively. 5% [Mooney et al., 1983; Chiu et al., 1992; Catchings, 1999], corresponding to a possible error of less than 3 km in the resulting H, and less than 0.01 in the Vp/Vs determinations.

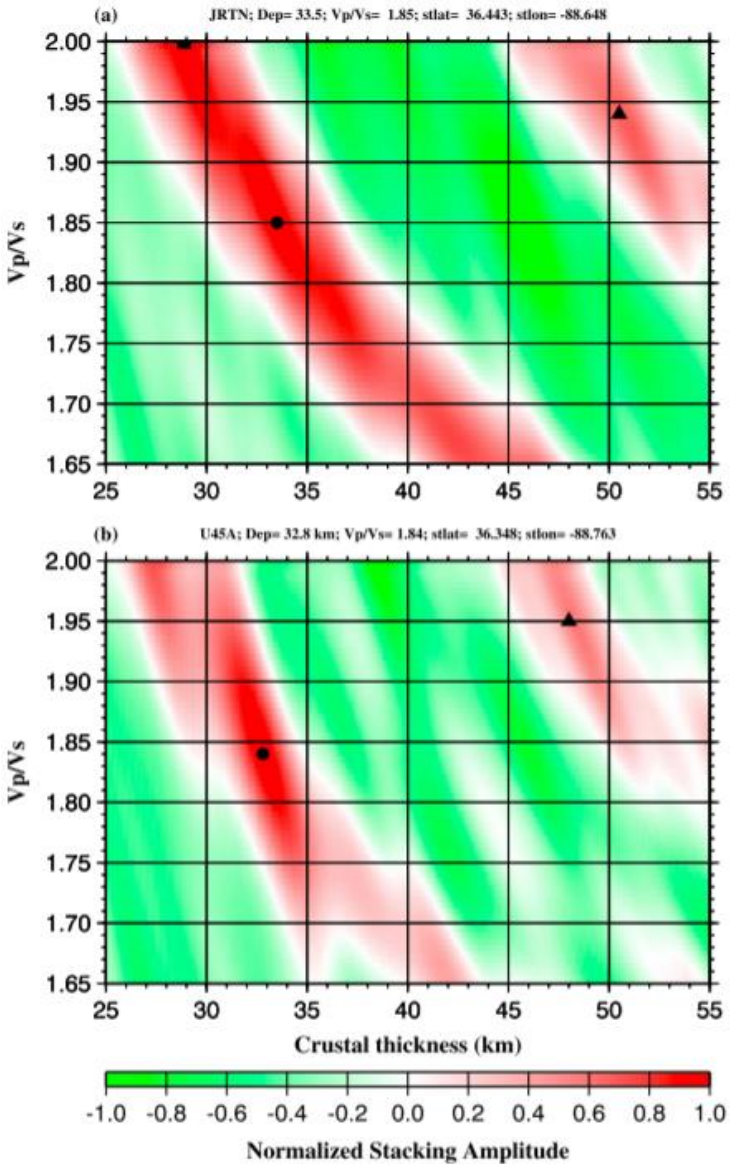

Figure 4. Image of stacking energy from H-κ stacking using the filtered RFs from stations JRTN and U45A located in the UME. The black dots and triangles show points with the first and second largest stacking amplitudes, corresponding to the top and bottom of a lower crustal layer, respectively.

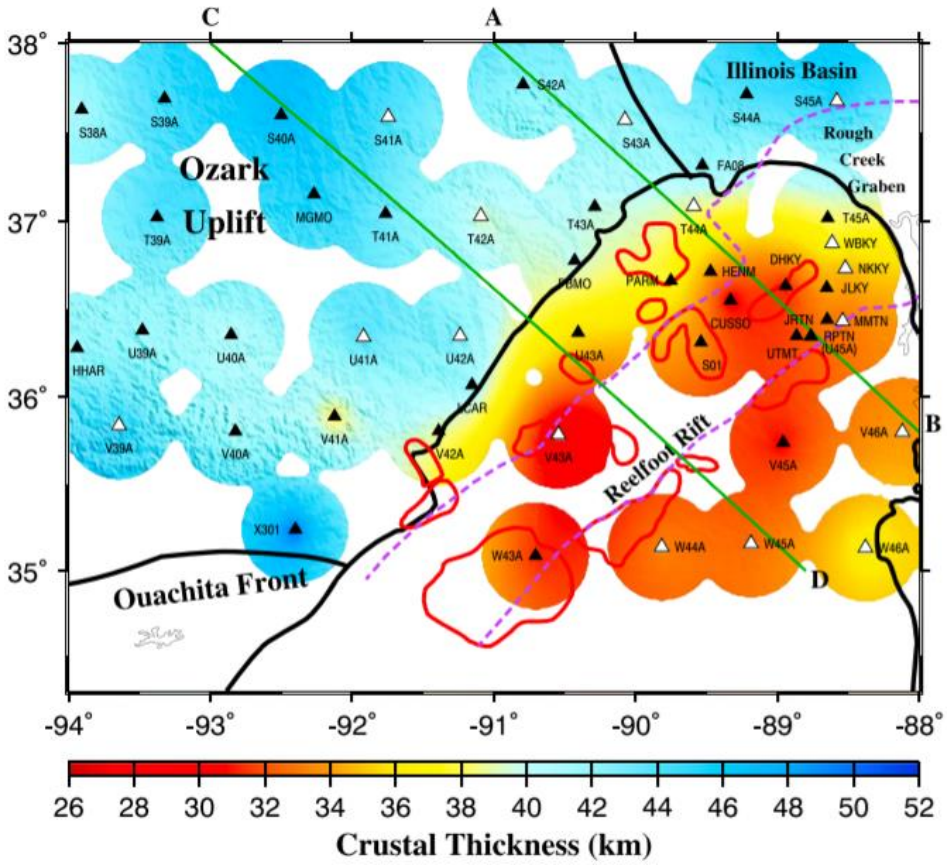

Figure 5. Resulting thickness of the crustal layer corresponding to the maximum stacking amplitude. Filled triangles are category A stations, and open triangles are category B stations. To produce the plot, the observations are fitted using a surface gridding algorithm [Wessel and Smith, 1991]. Only areas that are 40 km or closer to a station are shown. Lines A-B and C-D are the locations of the gravity model shown in Figures 7 and 8, respectively.

The Bouguer gravity anomaly data consisting of over 69,000 measurement points were obtained from the National Geospatial and Imaging Agency, the United States Geological Survey, and detailed surveys by Larson and Mickus [2013] and Ives et al. [2014]. The average data spacing of the merged data set ranges from less than 1 km within the UME to 1–4 km elsewhere. The merged data set was processed into simple Bouguer gravity anomalies using the 1967 International Gravity formula [Morelli, 1976], sea level as a datum, and 2.67 g/cm3 as a reduction density.

3. RESULTS

3.1. RF STACKING RESULTS

The 49 stations with observable PmS phases on the RFs are divided into categories A and B (Table 1) according to the characteristics of the RFs [Nair et al., 2006]. Stations in category A show a clear PmS arrival in the time window of 4 to 8 s, at least one of the PPmS and PSmS arrivals, and a well-defined peak on the H-κ plot. For category B stations, only the PmS is observed, resulting in an ambiguous determination of H and Vp/Vs [Nair et al., 2006]. For these stations, Vp/Vs cannot be reliably determined, and to estimate the crustal thickness, we assume a constant Vp/Vs based on the average Vp/Vs of category A stations in the same tectonic province (1.85 for stations in the UME and 1.78 for those on the Ozark Uplift) to get the crustal thickness (H_n). Thirty-three stations belong to category A and 16 to category B. In the following discussions, the H measurements for category A and H_n measurements for category B stations are used to qualify crustal thicknesses. Note that due to the influence of the loose sedimentary layer and relatively high noise level suffered by stations on loose sediments, some stations in the UME did not lead to a sufficient number of RFs with clear PmS arrivals, even after the reverberation removal technique is applied to the RFs. They are not used in the study.

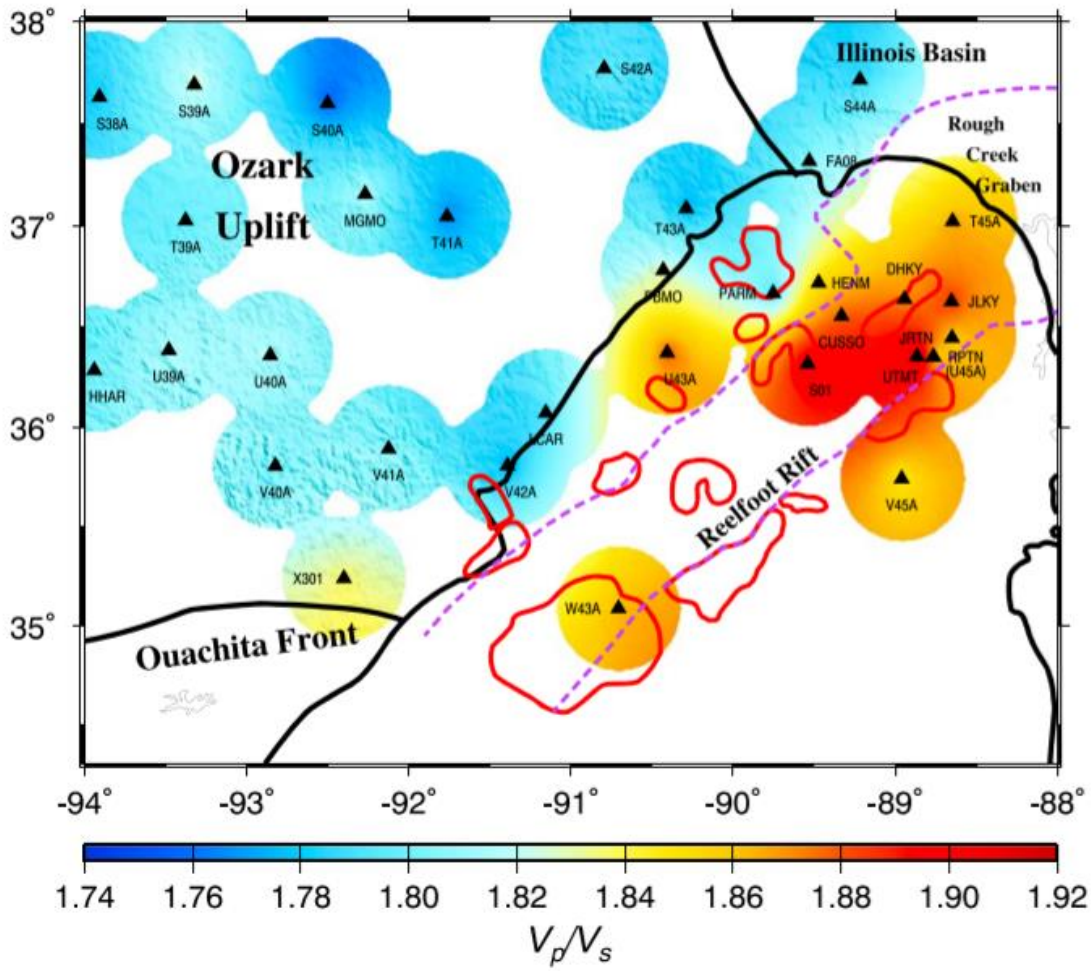

Figure 6. Resulting Vp/Vs measurements obtained at Category A stations.

The observed crustal thicknesses range from 26.8 to 50.3 km with a mean value of 38.4 ± 5.4 km (Figure 5), and the Vp/Vs observations of the 33 category A stations range from 1.75 to 1.93 with an average of 1.83 ± 0.04 (Figure 6). At the stations in the UME, the resulting thickness may not be that of the entire crust; instead, it may be the thickness of the upper crustal layer above a lower crustal layer with anomalously high density and seismic velocity. In other words, it is the vertical distance between the surface and an intracrustal interface. The bottom of the lower crustal layer is hinted in the H-κ plots of some of the stations in the NMSZ (Figure 4) and can also be represented by the deeper

arrival shown at most of the stations in the UME (Figures 7 and 8). This weaker interface has a depth of about 45–50 km, which is consistent with crustal thickness from seismic refraction studies [e.g., Mooney et al., 1983; Catchings, 1999]. The refraction studies also revealed an intracrustal layer at the depth of 25–30 km beneath the UME [see Catchings, 1999, Figures 8 and 9], a value that is comparable to the RF results (Figure 5).

3.1.1. Ozark Uplift. The crustal thickness measurements obtained using 4045 RFs from 22 stations on the Ozark Uplift range from 37.6 to 50.3 km with a mean value of 42.5 ± 3.0 km, and the Vp/Vs results range from 1.75 to 1.84 with a mean value of 1.80 ± 0.02 (Figures 5 and 6). The crustal thickness values are in general agreement with previous studies for this area [Chulick and Mooney, 2002; Ramírez-Guzmán et al., 2012; Hansen et al., 2015; McGlannan and Gilbert, 2016]. Both the crustal thickness and Vp/Vs results are typical for the North American cratonic areas [Keller, 2013].

3.1.2. UME and Illinois Basin. Almost all the stations in the UME are overlaid with unconsolidated Quaternary sediments, which lead to strong reverberations and a delayed first peak on the RFs (Figure 3a). After reverberation removal and manual checking, 2146 RFs from 24 stations are used for characterizing the crust beneath this area. As discussed earlier, the resulting depth from H-κ stacking represents most likely the top of the high-velocity lower crustal layer, except for a few stations at the edges of the areas. The resulting depths of the interface corresponding to the maximum stacking amplitude on the H-κ plots range from 26.8 to 40.0 km with an average of 33.9 ± 3.2 km, and the Vp/Vs values are between 1.79 and 1.93 with an average of 1.86 ± 0.03, suggesting a mafic composition [Christensen, 1996]. Another possible cause of the high Vp/Vs is partial melting of crustal rocks [Watanabe, 1993]. However, continental areas

with pervasive crustal partial melting are usually modern rift zones characterized by high heat flow, greatly thinned crust, negative gravity anomalies, and slower crustal seismic velocities (e.g., Reed et al. [2014] for the Afar Depression). These characteristics are generally not associated with the UME.

McGlannan and Gilbert [2016] conducted RF stacking by using a reference Vp of 6.6 km/s [Catchings, 1999] and a constant Vp/Vs value of 1.785. The resulting thicknesses corresponding to the largest stacking amplitude are 5–10 km greater than those of ours in this area (Figures 2 and 5). The discrepancy is most likely caused by the different reference P wave velocities. Increasing Vp by 8% (from 6.1 to 6.6 km/s) would increase the resulting crustal thickness by nearly 3.7 km. In addition, assuming a Vp/Vs of 1.785 instead of 1.85 can further increase the resulting H by approximately 4 km [Nair et al., 2006].

The southernmost portion of the Illinois Basin is sampled by 1436 RFs recorded at three stations. The observed crustal thicknesses range from 42.0 to 45.9 km, while the Vp/Vs values are from 1.78 to 1.81. The average crustal thickness is 44.0 ± 1.9 km, and the mean Vp/Vs value is 1.80 ± 0.02, which is comparable to those observed on the Ozark Uplift but is smaller than those obtained in the UME. The measured crustal thicknesses of Ramírez-Guzmán et al. [2012], Chen et al. [2014], Pollitz and Mooney [2014], andMcGlannan and Gilbert [2016] are approximately 40 km beneath the southernmost part of the Illinois Basin, while those of Hansen et al. [2015] are greater than 45 km. Therefore, results from this study are in general agreement with those from previous studies.

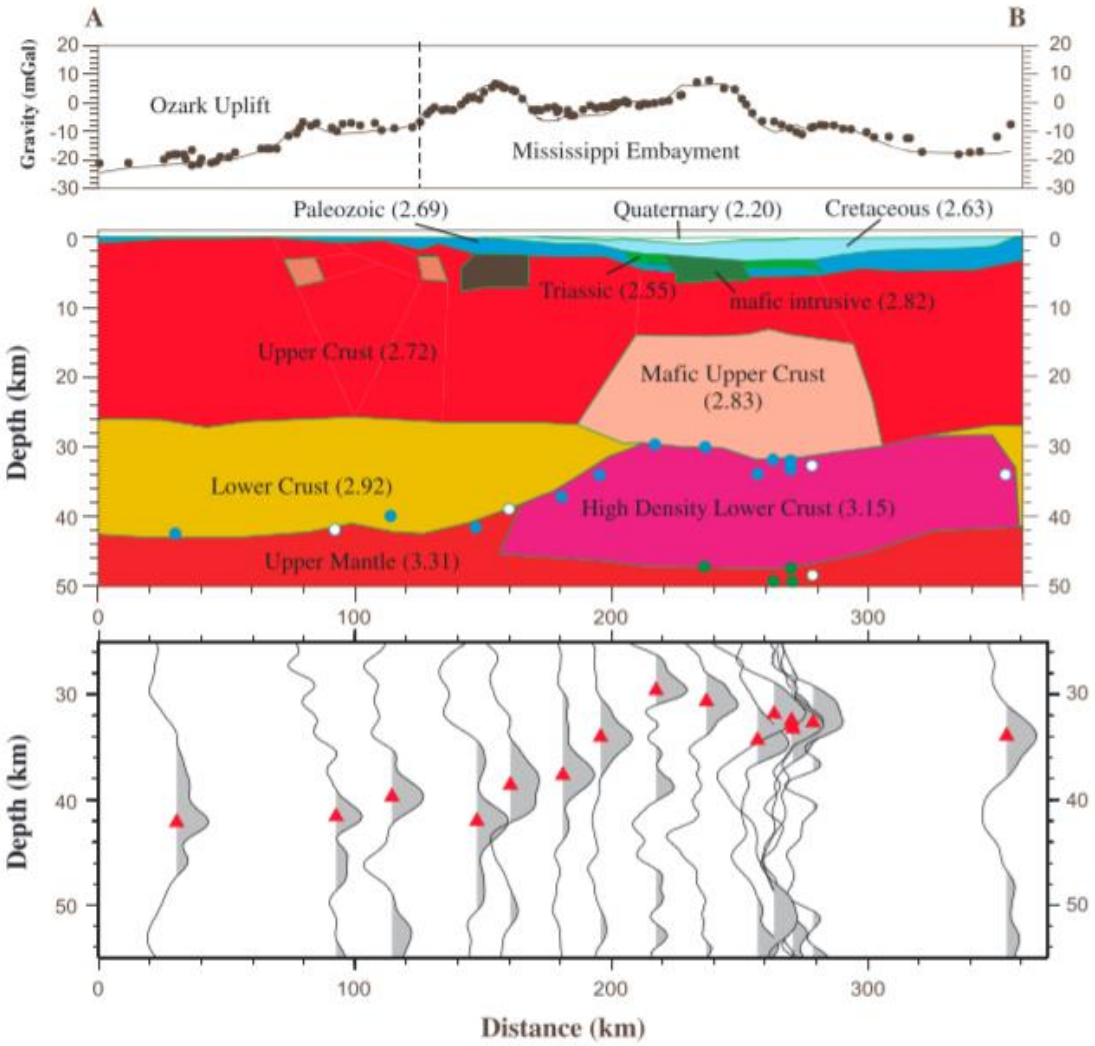

Figure 7. Gravity model of the crust and uppermost mantle and stacked RFs along profile A-B (Figure 5). Densities are in g/cm3. (top) Observed (black dots) and calculated (solid line) Bouguer gravity anomalies. (middle) Resulting gravity model. Blue circles represent the depth of the arrival on the H-κ plots with the largest stacking amplitude at stations in a 100 km wide band centered on the profile, filled circles are category A stations, open circles are category B stations, and green circles are the approximate depths of the deeper secondary arrival. (bottom) Stacked and depth-converted RFs using the resulting Vp/Vs corresponding to the maximum stacking amplitude on the H-κ plot for each of the stations.

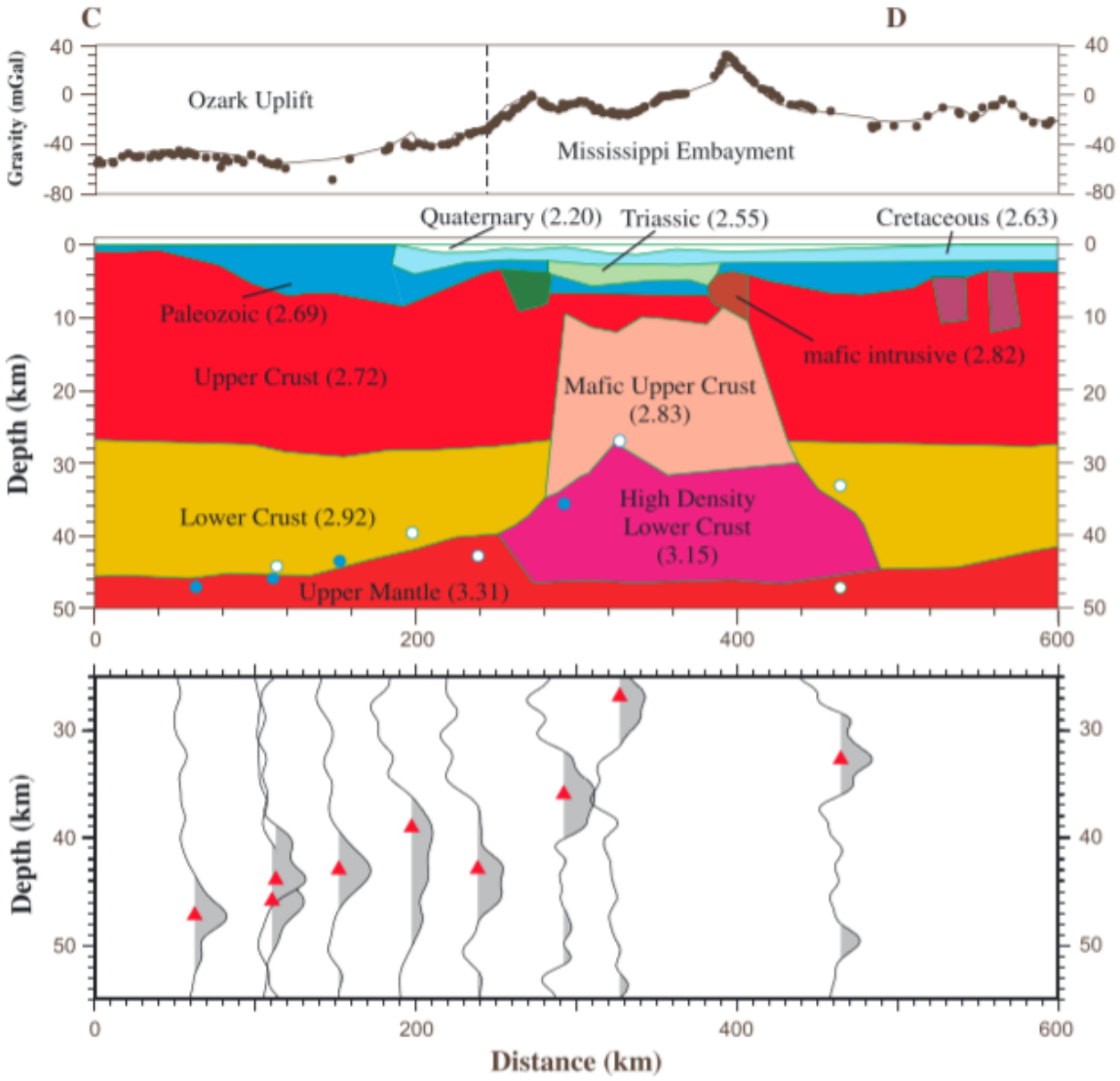

Figure 8. Same as Figure 7 but along profile C-D.

3.2. GRAVITY MODELING RESULTS

Modeling of Bouguer gravity anomalies can aid in constraining the crustal structures determined from the seismic results and provide a more detailed image of the upper crustal layer than that determined from broadband seismic modeling [e.g., Bashir et al., 2011; England and Ebbing, 2012; Yu et al., 2015b; Schiffer et al., 2016]. Two models along profiles A-B and C-D (Figure 5) were constructed. The forward modeling of the

observed Bouguer gravity anomaly data (Figures 7 and 8) was constrained by seismic refraction modeling [Mooney et al., 1983], previous gravity and magnetic analysis [Hildenbrand, 1985], and the resulting crustal thickness and Vp/Vs results from the H-κ stacking (Figures 5 and 6) in this study. The H-κ stacking results from this study were used to model the crustal thickness or the thickness of the upper crustal layer beneath the UME. The seismic refraction models [Mooney et al., 1983] were used to constrain the upper crustal geometries, while previous gravity and magnetic studies [Hildenbrand, 1985] were applied to estimate the location of the mafic intrusions. The P wave velocities from the seismic refraction models of Mooney et al. [1983] were converted to densities and used as starting values for the densities in each of the bodies shown in the gravity models. The densities were then varied by a maximum of 15% in order for the calculated gravity values to match the observed gravity anomalies.

The resulting Bouguer gravity anomaly models along profiles A-B and C-D (Figures 7 and 8) are consistent with the existence of both a high-density upper crustal layer and a higher-density lower crustal layer beneath the UME. Like many other continental rifts [Thybo and Artemieva, 2013] such as the Baikal [Thybo and Nielsen, 2009] and East African rifts [Birt et al., 1997], the Reelfoot Rift is characterized by an upper crustal graben and an altered lower crustal layer [Mooney et al., 1983; Catchings, 1999; Ramírez-Guzmán et al., 2012], and the existence of the high-density upper crustal layer is consistent with the distribution of the relatively high Vp/Vs values (Figure 6).

It is well known that gravity modeling is non-unique. During the modeling process a number of different models were created to determine this non-uniqueness. The gravity modeling alone could not determine the exact thicknesses and densities of the

crustal layers nor could it determine if a high-density upper crustal body was required. However, if the high-density upper crustal layer was not modeled, then the crust was thinner (~40 km) than observed under the UME. While this model does roughly fit the available constraints, including the high-density crustal body better explains the high Vp/Vs measurements, and the resulting thicknesses are more consistent with the RF and seismic refraction results.

4. DISCUSSION

4.1. MAFIC INTRUSION INTO THE UPPER CRUSTAL LAYER BENEATH THE UME

The bulk properties of the crust can be determined by the resulting crustal thickness and Vp/Vs measurements. It is commonly accepted that felsic, intermediate, and mafic rocks have typical Vp/Vs values of smaller than 1.78, between 1.78 and 1.81, and greater than 1.81, respectively [Christensen, 1996]. The laboratory measurements made by Christensen [1996] also concluded that the average Vp/Vs is approximately 1.74 and 1.81 in the upper and lower crust, respectively, with an average value of 1.78 for the entire continental crust.

The UME is located within the granite-rhyolite provinces [Van Schmus, 1992], where the crust was pervasively modified by granitic and associated anorthitic intrusions during the Proterozoic [Whitmeyer and Karlstrom, 2007]. As granite is a felsic rock and has a low Vp/Vs value of 1.71, the high Vp/Vs observed beneath the UME most likely reflects intrusion of mafic material into the upper crust. We argue that the mafic intrusion took place during the Cretaceous time, mostly because of the fact that the vast majority of mafic intrusions found near the surface are Cretaceous in age [Hildenbrand and Hendricks, 1995], and thus, it is reasonable to assume that mafic intrusions of the same age also exist deep in the crust.

One of the new findings from this study is the likely existence of a mafic high-density upper crustal layer beneath the UME sampled by the broadband seismic stations (Figure 6). Unlike the mafic lower crustal layer which has been identified beneath almost all continental rifts [Mooney et al., 1983; Keller et al., 2006; Thybo and Nielsen, 2009;

Birt et al., 1997], the existence of a mafic upper crustal layer is rare, if not previously unrecognized, for continental rifts, and might be responsible for the second phase of subsidence the studied UME area has experienced since the Cretaceous through isostatic adjustment.

4.2. CONSTRAINTS ON SUBSIDENCE MODELS

Among the proposed mechanisms for the second phase of subsidence of the UME, including far-field regional extensional stress [Ervin and McGinnis, 1975; Kane et al., 1981], episodic variations in lithospheric viscosity due to increased geothermal gradient [DeRito et al., 1983; Braile et al., 1986], and the thermal-elastic effects of a passing mantle plume [Van Arsdale and Cox, 2007], the passage of the proposed Bermuda mantle plume is arguably most capable of inducing pervasive igneous intrusions into both the upper and lower crustal layers along previous fractured zones of weakness produced by the initial rifting in the Late Precambrian. This model can also explain the ~2 km uplift of the UME during the Cretaceous [Van Arsdale and Cox, 2007; Hildenbrand et al., 1996; Cox and Van Arsdale, 2002]. The model further suggests that the plume heated the continental lithosphere, causing it to expand and rise to form an arch which was then eroded to low relief. When the area moved off of the plume, the heavier-than-normal UME crust cooled and sank starting from the Late Cretaceous. The surface was lowered below sea level, resulting in a depression that allowed water from the Gulf of Mexico to invade the area [Van Arsdale and Cox, 2007].

It should be pointed out that while our observations are in agreement with the predictions of a passing plume model, the existence of such a plume during the Mesozoic

beneath our study area was solely based on conclusions from some of the previous studies. Similar to most other perceived mantle plumes, the origin of the igneous rocks in the UME remains enigmatic, and seismological observations regarding whether the recent Bermuda volcanism is associated with a lower mantle plume, a plume originated in the mantle transition zone, or edge-driven small-scale convection is a debated topic, which requires additional interdisciplinary studies to possibly resolve [Benoit et al., 2013; Gao and Liu, 2014].

4.3. EFFECT OF THE POSSIBLE THERMAL UPWELLING ON THE OZARK UPLIFT

In comparison with the spatial variation of crustal thickness and Vp/Vs measurements in the central U.S. [Chulick and Mooney, 2002; Keller, 2013], especially the midcontinental cratonic region to the north of the study area, our observations (42.5 ± 3.0 km and 1.80 ± 0.02) beneath the Ozark Uplift are normal values. Corresponding to the negative Bouguer gravity anomalies and felsic upper crustal layer in our gravity modeling (Figures 7 and 8), a low-density granitic upper crustal layer is implied and can be explained as being derived from the Proterozoic granite-rhyolite intrusion event [Hildenbrand et al., 1996]. Although mafic intrusions occurred beneath the UME, it is apparent that the thermal upwelling could not penetrate the strong cratonic lithosphere of the Ozark Uplift [Cox and Van Arsdale, 2002]. The difference in the influence of the passing plume might suggest that the plume could only significantly affect areas of weakness of the continental lithosphere, and the strong cratonic lithosphere can prevent major intrusion, so the crust is essentially unmodified by the passing plume.

5. CONCLUSIONS

Observations of crustal properties measured using RFs and gravity anomaly data confirm the existence of a mafic, high-density lower crustal layer beneath the UME, and reveal a high-density mafic upper crustal layer which is not commonly found beneath other continental rifts. The previously inferred dominantly Cretaceous age of the mafic intrusions found in the UME and the approximately 2 km rise of the area preceding the post-Cretaceous subsidence suggest a possible role of a passing mantle plume on the tectonic evolution of the UME. Intrusion of mantle material into the UME crust fractured by rifting during the Late Precambrian increased the bulk density of the crust, leading to renewed subsidence after the plume moved away from the area. The Ozark Uplift, in contrast, is characterized by normal crustal thickness and Vp/Vs measurements that are similar to those of midcontinent cratonic crust, suggesting that the plume did not penetrate the strong and thick lithosphere beneath the Ozark Uplift.

REFERENCES

Ammon, C. J. (1991), The isolation of receiver effects from teleseismic P waveforms, Bull. Seismol. Soc. Am., 81, 2504–2510.

Bashir, L., S. S. Gao, K. H. Liu, and K. Mickus (2011), Crustal structure and evolution beneath the Colorado Plateau and the southern Basin and Range Province: Results from receiver function and gravity studies, Geochem. Geophys. Geosyst., 12, 1525–2027, doi:10.1029/2011GC003563.

Benoit, M. H., M. D. Long, and S. D. King (2013), Anomalously thin transition zone and apparently isotropic upper mantle beneath Bermuda: Evidence for upwelling, Geochem. Geophys. Geosyst., 14, 4282–4291, doi:10.1002/ggge.20277.

Birt, C. S., P. K. H. Maguire, M. A. Khan, H. Thybo, G. R. Keller, and J. Patel (1997), The influence of pre-existing structures on the evolution of the southern Kenya Rift valley: Evidence from seismic and gravity studies, Tectonophysics, 278, 211–242.

Braile, L. W., W. J. Hinze, G. R. Keller, E. G. Lidiak, and J. L. Sexton (1986), Tectonic development of the New Madrid rift complex, Mississippi embayment, North America, Tectonophysics, 131, 1–21, doi:10.1016/0040-1951(86)90265-9.

Catchings, R. D. (1999), Regional Vp, Vs, Vp/Vs, and Poisson's ratios across earthquake source zones from Memphis, Tennessee, to St. Louis, Missouri, Bull. Seismol. Soc. Am., 89, 1591–1605.

Chen, C., D. Zhao, and S. Wu (2014), Crust and upper mantle structure of the New Madrid Seismic Zone: Insight into intraplate earthquakes, Phys. Earth Planet. Inter., 230, 1–14, doi:10.1016/j.pepi.2014.01.016.

Chiu, J. M., A. C. Johnston, and Y. T. Yang (1992), Imaging the active faults of the central New Madrid seismic zone using PANDA array data, Seismol. Res. Lett., 63, 375–393, doi:10.1785/gssrl.63.3.375.

Christensen, N. I. (1996), Poisson's ratio and crustal seismology, J. Geophys. Res., 101, 3139–3156, doi:10.1029/95JB03446.

Christensen, N. I., and W. D. Mooney (1995), Seismic velocity structure and composition of the continental crust: A global view, J. Geophys. Res., 100, 9761–9788, doi:10.1029/95JB00259.

Chulick, G. S., and W. D. Mooney (2002), Seismic structure of the crust and uppermost mantle of North America and adjacent oceanic basins: A synthesis, Bull. Seismol. Soc. Am., 92, 2478–2492, doi:10.1785/0120010188.

Cox, R. T., and R. B. Van Arsdale (1997), Hotspot origin of the Mississippi embayment and its possible impact on contemporary seismicity, Eng. Geol., 46, 201–216, doi:10.1016/S0013-7952(97)00003-3.

Cox, R. T., and R. B. Van Arsdale (2002), The Mississippi Embayment, North America: A first order continental structure generated by the Cretaceous superplume mantle event, J. Geodyn., 34, 163–176, doi:10.1016/S0264-3707(02)00019-4.

Dart, R. L., and H. S. Swolfs (1998), Contour mapping of relic structures in the Precambrian basement of the Reelfoot rift, North American midcontinent, Tectonics, 17, 235–249.

DeRito, R. F., F. A. Cozzarelli, and D. S. Hodge (1983), Mechanism of subsidence of ancient cratonic rift basins, Tectonophysics, 94, 141–168, doi:10.1016/0040-1951(83)90014-8.

England, R. W., and J. Ebbing (2012), Crustal structure of central Norway and Sweden from integrated modelling of teleseismic receiver functions and the gravity anomaly, Geophys. J. Int., 191, 1–11, doi:10.1111/j.1365-246X.2012.05607.x.

Ervin, C. P., and L. D. McGinnis (1975), Reelfoot rift: Reactivated precursor to the Mississippi embayment, Geol. Soc. Am. Bull., 86, 1287–1295, doi:10.1130/0016-7606(1975)862.0.CO;2.

Gao, S. S., and K. H. Liu (2014), Mantle transition zone discontinuities beneath the contiguous United States, J. Geophys. Res. Solid Earth, 119, 6452–6468, doi:10.1002/2014JB011253.

Hansen, S. M., K. Dueker, and B. Schmandt (2015), Thermal classification of lithospheric discontinuities beneath USArray, Earth Planet. Sci. Lett., 431, 36–47, doi:10.1016/j.epsl.2015.09.009.

Hildenbrand, T. G. (1985), Rift structure of the northern Mississippi embayment from the analysis of gravity and magnetic data, J. Geophys. Res., 90, 12,607–12,622, doi:10.1029/JB090iB14p12607.

Hildenbrand, T. G., and J. D. Hendricks (1995), Geophysical setting of the Reelfoot rift and relations between rift structures and the New Madrid seismic zone, US Geol. Surv. E1538, U.S. Geol. Surv., Washington, D. C.

Hildenbrand, T. G., A. Griscom, W. R. Van Schmus, and W. D. Stuart (1996), Quantitative investigations of the Missouri gravity low: A possible expression of a large, Late Precambrian batholith intersecting the New Madrid seismic zone, J. Geophys. Res., 101, 21,921–21,942, doi:10.1029/96JB01908.

Ives, B., K. Mickus, A. McCafferty, C. Seeger, and M. Starkey (2014), Analyzing the Paleozoic basement structure and lithologies of the northwest St. Francois Terrance, Missouri using gravity data to investigate possible mineral deposits of economic interest, Geol. Soc. Am. Abstr. Programs, 46, 308.

Kane, M. F., T. G. Hildenbrand, and J. D. Hendricks (1981), Model for the tectonic evolution of the Mississippi Embayment and its contemporary seismicity, Geology, 9, 563–568, doi:10.1130/0091-7613(1981).9.2.0.CO;2.

Keller, G. R. (2013), The Moho of North America: A brief review focused on recent studies, Tectonophysics, 609, 45–55, doi:10.1016/j.tecto.2013.07.031.

Keller, G. R., M. A. Khan, P. Morgan, R. F. Wendlandt, W. S. Baldridge, K. H. Olsen, C. Prodehl, and L. W. Braile (1991), A comparative study of the Rio Grande and Kenya rifts, Tectonophysics, 197, 355–371.

Keller, G. R., R. F. Wendlandt, and M. H. P. Bott (2006), West and central African rift system, Dev. Geotectonics, 25, 437–449.

Kennett, B. L. N., and E. R. Engdahl (1991), Traveltimes for global earthquake location and phase identification, Geophys. J. Int., 105, 429–465.

Langston, C. A. (1977), The effect of planar dipping structure on source and receiver responses for constant ray parameter, Bull. Seismol. Soc. Am., 67, 1029–1050.

Larson, M., and K. Mickus (2013), Gravity and magnetic analysis of plutons, ring plutons and mafic bodies in the St. Francois Mountains, SE Missouri, Geol. Soc. Am. Abstr. Programs, 45, 2.

Liang, C., and C. A. Langston (2009), Three-dimensional crustal structure of eastern North America extracted from ambient noise, J. Geophys. Res., 114, B03310, doi:10.1029/2008JB005919.

Liu, K. H., and S. S. Gao (2010), Spatial variations of crustal characteristics beneath the Hoggar swell, Algeria, revealed by systematic analyses of receiver functions from a single seismic station, Geochem. Geophys. Geosyst., 11, Q08011, doi:10.1029/2010GC003091.

Logatchev, N. A., and N. A. Florensov (1978), The Baikal system of rift valleys, Tectonophysics, 45, 1–13.

McCamy, K., and R. P. Meyer (1966), Crustal results of fixed multiple shots in the Mississippi embayment, in The Earth Beneath the Continents, edited by J. S. Steinhart and T. J. Smith, pp. 370–381, AGU, Washington, D. C., doi:10.1029/GM010p0370.

McGlannan, A. J., and H. Gilbert (2016), Crustal signatures of the tectonic development of the North American midcontinent, Phys. Earth Planet. Inter., 433, 339–349, doi:10.1016/j.epsl.2015.10.048.

Mooney, W. D., M. C. Andrews, A. Ginzburg, D. A. Peters, and R. M. Hamilton (1983), Crustal structure of the northern Mississippi embayment and a comparison with other continental rift zones, Tectonophysics, 94, 327–348, doi:10.1016/0040-1951(83)90023-9.

Morelli, C. (1976), Modern standards for gravity surveys, Geophysics, 41, 1051, doi:10.1190/1.1440661.

Nair, S. K., S. S. Gao, K. H. Liu, and P. G. Silver (2006), Southern African crustal evolution and composition: Constraints from receiver function studies, J. Geophys. Res., 111, B02304, doi:10.1029/2005JB003802.

Pollitz, F. F., and W. D. Mooney (2014), Seismic structure of the central US crust and shallow upper mantle: Uniqueness of the Reelfoot Rift, Earth Planet. Sci. Lett., 402, 157–166, doi:10.1016/j.epsl.2013.05.042.

Ramírez-Guzmán, L., O. S. Boyd, S. Hartzell, and R. A. Williams (2012), Seismic velocity model of the central United States (version 1): Description and simulation of the 18 April 2008 Mt. Carmel, Illinois, earthquake, Bull. Seismol. Soc. Am., 102, 2622–2645, doi:10.1785/0120110303.

Reed, C. A., S. Almadani, S. S. Gao, A. A. Elsheikh, S. Cherie, M. G. Abdelsalam, A. K. Thurmond, and K. H. Liu (2014), Receiver function constraints on crustal seismic velocities and partial melting beneath the Red Sea rift and adjacent regions, Afar Depression, J. Geophys. Res. Solid Earth, 119, 2138–2152, doi:10.1002/2013JB010719.

Schiffer, C., N. Balling, J. Ebbing, B. H. Jacobsen, and S. B. Nielsen (2016), Geophysical-petrological modelling of the East Greenland Caledonides—Isostatic support from crust and upper mantle, Tectonophysics, 692, 44–57, doi:10.1016/j.tecto.2016.06.023.

Schwalb, H. R. (1969), Paleozoic geology of the Jackson Purchase region, Kentucky: Kentucky Geol. Surv. Rep. of Invest., 10, 40.

Stewart, S. W. (1968), Crustal structure in Missouri by seismic-refraction methods, Bull. Seismol. Soc. Am., 58, 291–323.

Thomas, W. A. (1991), The Appalachian-Ouachita rifted margin of southeastern North America, Geol. Soc. Am. Bull., 103, 415–431, doi:10.1130/0016-7606(1991)1032.3.CO;2.

Thybo, H., and I. M. Artemieva (2013), Moho and magmatic underplating in continental lithosphere, Tectonophysics, 609, 605–619.

Thybo, H., and C. A. Nielsen (2009), Magma-compensated crustal thinning in continental rift zones, Nature, 457, 873–876, doi:10.1038/nature07688.

Van Arsdale, R. B., and R. T. Cox (2007), The Mississippi's curious origins, Sci. Am., 296, 76–82.

Van Schmus, W. R. (1992), Tectonic setting of the midcontinent rift system, Tectonophysics, 213, 1–15, doi:10.1016/0040-1951(92)90247-4.

Watanabe, T. (1993), Effects of water and melt on seismic velocities and their application to characterization of seismic reflectors, Geophys. Res. Lett., 20, 2933–2936.

Wessel, P., and W. H. Smith (1991), Free software helps map and display data, Eos Trans. AGU, 72, 441–446.

Whitmeyer, S. J., and K. E. Karlstrom (2007), Tectonic model for the Proterozoic growth of North America, Geosphere, 3, 220–259, doi:10.1130/GES00055.1.

Yu, Y., J. Song, K. H. Liu, and S. S. Gao (2015a), Determining crustal structure beneath seismic stations overlying a low-velocity sedimentary layer using receiver functions, J. Geophys. Res. Solid Earth, 120, 3208–3218, doi:10.1002/2014JB011610.

Yu, Y., K. H. Liu, C. A. Reed, M. Moidaki, K. Mickus, E. A. Atekwana, and S. S. Gao (2015b), A joint receiver function and gravity study of crustal structure beneath the incipient Okavango Rift, Botswana, Geophys. Res. Lett., 42, 8398–8405, doi:10.1002/2015GL065811.

Zelt, B. C., and R. M. Ellis (1999), Receiver-function studies in the Trans-Hudson orogen, Saskatchewan, Can. J. Earth Sci., 36, 585–603, doi:10.1139/cjes-36-4-585.

Zhu, L., and H. Kanamori (2000), Moho depth variation in southern California from teleseismic receiver functions, J. Geophys. Res., 105, 2969–2980, doi:10.1029/1999JB900322.

II. LITHOSPHERIC LAYERING BENEATH THE CONTIGUOUS UNITED STATES CONSTRAINED BY S-TO-P RECEIVER FUNCTIONS

ABSTRACT

To image upper mantle seismic discontinuities beneath the contiguous United States, a total of 284,121 S-to-P receiver functions (SRFs) recorded by 3,594 broadband seismic stations in the EarthScope Transportable Array and other permanent and temporary deployments are common-conversion-point (CCP) stacked in circular bins of 2° 11 in radius. A robust negative arrival, representing a sharp discontinuity of velocity reduction with depth, is visible in virtually all the CCP stacked traces in the depth range of 30-110 km. Beneath the western U.S., the mean depth of this discontinuity is 69 ± 17 km, and beneath the eastern U.S., it is 76 ± 5 km, both of which are comparable to the depth of the tomographically-determined lithosphere asthenosphere boundary (LAB). In contrast, the depth of the discontinuity beneath the stable cratonic region of the central U.S. is 87 ± 6 km, which is significantly shallower than the ~250 km LAB depth determined by seismic tomography. Based on the amplitude of the corresponding arrival in the SRFs and findings from previous seismic tomography and mantle xenolith studies, this discontinuity beneath the central U.S. is interpreted as the top of an intra-lithospheric low-velocity, probably phlogopite-rich layer. The observations also provide new constraints on a number of regional scale tectonic processes, such as lithospheric stretching in the Texas-Louisiana Gulf Coastal Plain and Basin and Range Province, and possible lithospheric basal erosion beneath the northeastern U.S.

1. INTRODUCTION

Reliably mapping the thickness and layering of the lithosphere, which is the outermost rigid shell of the Earth, is essential in understanding upper mantle structure and dynamics (Chen, 2017). Two of the most frequently employed seismological techniques for investigating lithospheric thickness and layering are surface wave tomography (Bedle and van der Lee, 2009; Calò et al., 2016) and common-conversion-point (CCP) stacking of receiver functions which are P-to-S or S-to-P converted phases (Ps and Sp, respectively) from velocity discontinuities at the bottom of or inside the lithosphere (Fischer et al., 2010; Kind et al., 2012). Surface wave tomography can detect gradual variations in velocity gradient, but is insensitive to sharp discontinuities due to low vertical resolution (Li et al., 2007; Rychert et al., 2007). In contrast, P-to-S receiver functions are widely used for imaging the Moho and mantle transition zone discontinuities (Zhu and Kanamori, 2000; Liu et al., 2017; Gao and Liu, 2014), but are not effective to study lithospheric discontinuities because of the strong Moho multiples in the expected time window of the arrivals associated with the discontinuities (Faber and Müller, 1980). Instead, lithospheric discontinuities are commonly imaged using S-to-P receiver functions 48 (SRFs), in which the Sp arrivals are precursors to the direct S-wave. Because the Moho multiples appear after the direct S-wave, a separation of the primary converted phases and the multiples is expected on the SRFs (Faber and Müller, 1980). Relative to surface wave tomography, SRF stacking has the disadvantage that only sharp discontinuities can be detected. Tests suggest that a discontinuity that is 50 km or thicker cannot generate observable S-to-P converted phases (Kumar et al., 2012).

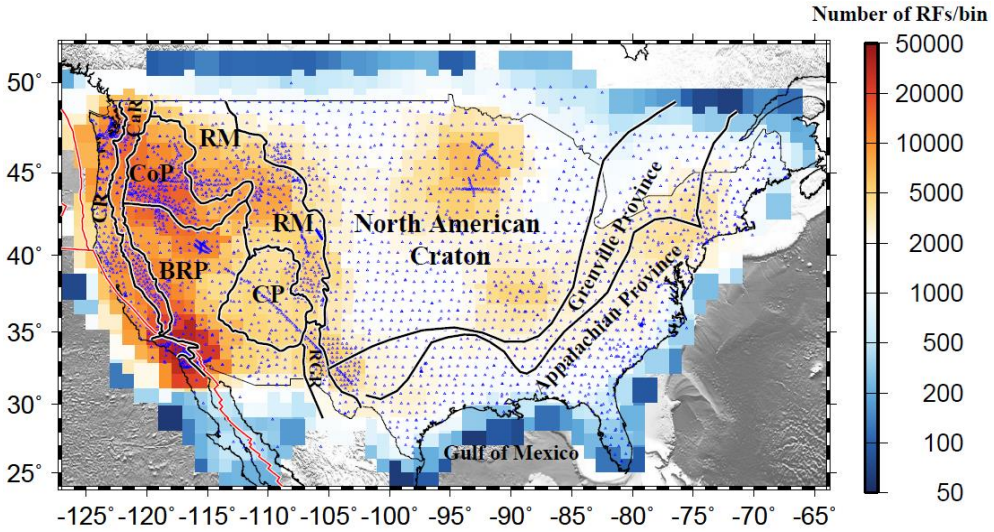

Figure 1. Number of S receiver functions in radius = 2° circular bins and broadband seismic stations (blue triangles) used in the study. The thick black lines delineate major tectonic provinces CR: Coast Ranges, CaR: Cascade Range-Sierra Nevada, CoP: Columbia Plateau, BRP: Basin and Range Province, RM: Rocky Mountains, CP: Colorado Plateau, and RGR: Rio Grande Rift (Hoffman, 1988).

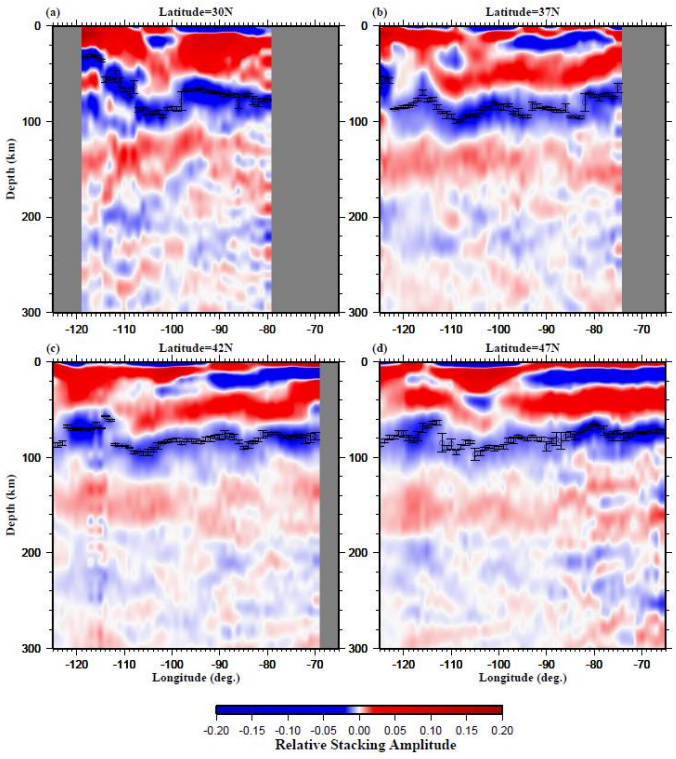

Figure 2. Example plots of cross-sections along four latitudinal lines. The black circles mark the picked depth of the NVD. Similar plots for all the 27 latitudinal lines can be found in Fig. S1.

Beneath the contiguous United States, the observed lithospheric thickness from most surface wave tomography studies demonstrates similar spatial variations, with values as small as less than 70 km beneath the western U.S., 90-150 km along the Rocky Mountains, Colorado Plateau, and Appalachians, and about 250 km beneath the tectonically stable cratonic region of the central U.S. (Bedle and van der Lee, 2009; Schaeffer and Lebedev, 2014). The observed spatial variations of lithospheric thickness correspond well with measurements from shear wave velocity gradient (Yuan and Romanowicz, 2010), electrical conductivity (Murphy and Egbert, 2017), mantle xenolith (Mareschal and Jaupart, 2004), and shear wave splitting (Yang et al., 2014).

A number of SRF studies have been conducted over the past decade to image lithospheric discontinuities beneath North America (Li et al., 2007; Rychert et al., 2007; Abt et al., 2010; Kind et al., 2012; Kumar et al., 2012; Levander and Miller, 2012; Lekić and Fischer, 2014; Hansen et al., 2015; Hopper and Fischer, 2015; Reeves et al., 2015). Most previous work report a sharp negative-velocity discontinuity (NVD) in the depth range of 40-180 km beneath the contiguous U.S. The NVD beneath the western and eastern U.S. has a depth ranging 73 from 40 to 110 km, which is similar to the depth of the lithosphere-asthenosphere boundary (LAB) revealed by surface wave tomography, and is consequently considered as the bottom of the lithosphere (Rychert et al., 2007; Abt et al., 2010; Hansen et al., 2015). In contrast, the depth of the NVD beneath the central U.S. ranges from 80 to 180 km (Kumar et al., 2012; Hansen et al., 2015), which is significantly smaller than the ~250 km depth determined using surface wave tomography (Bedle and van der Lee, 2009; Schaeffer and Lebedev., 2014). The NVD is therefore

regarded as a mid-lithospheric discontinuity (MLD) rather than the LAB beneath most areas of the central U.S.

The current study is motivated by a number of factors. First, previous SRF CCP studies used only a portion of the EarthScope Transportable Array (TA) stations, leading to limited station coverage especially for the eastern U.S. Second, there are apparent discrepancies among existing SRF investigations in the resulting depth of the NVD (see Figure 8 in Hansen et al., 2015 for a comparison of results from four SRF studies). For instance, in the stable cratonic region of the central U.S., the depth is ~100 km in Abt et al. (2010), Kumar et al. (2012), Foster et al. (2014) and Hopper and Fischer (2015), but is as large as 160 km in Hansen et al. (2015). Such discrepancies are most likely caused by the weak signal from the target discontinuities and the consequent uncertainties in reliably identifying the correct arrivals, especially when a small bin size for stacking is used to reach a high lateral resolution (e.g., the radius is about 0.4° in Hansen et al., 2015). In this study, we use a relatively large bin size (radius=2°) to obtain more reliable results with a comparatively lower resolution for the whole contiguous U.S. Third, while it is 98 known that the stacking amplitude of the negative arrival from the NVD is a significant parameter to quantify the sharpness of the interface to provide additional constraints on the nature of the discontinuities (Abt et al., 2010), spatial variation of the amplitude over the entire study area is still lacking. Finally, some of the SRF studies (Li et al., 2007; Kumar et al., 2012; Hansen et al., 2015) briefly discussed the possibility that the negative arrival beneath the Moho could be a side-lobe of the strong S-to-P conversion from the Moho. Although this possibility has been considered as unlikely based on the strong amplitude of the negative arrival and the occasionally independent

structure of the Moho and the NVD, a systematic synthetic study to confirm this is still lacking.

In this study we use all the available broadband seismic data recorded prior to January, 2016, including those from all the TA stations, to image the depth of and SRF stacking amplitude associated with lithospheric discontinuities beneath the contiguous U.S., with an unprecedented station coverage for the area. Additionally, we perform synthetic test on the possibility that the observed negative arrival corresponding to the NVD is an artifact from the Moho.

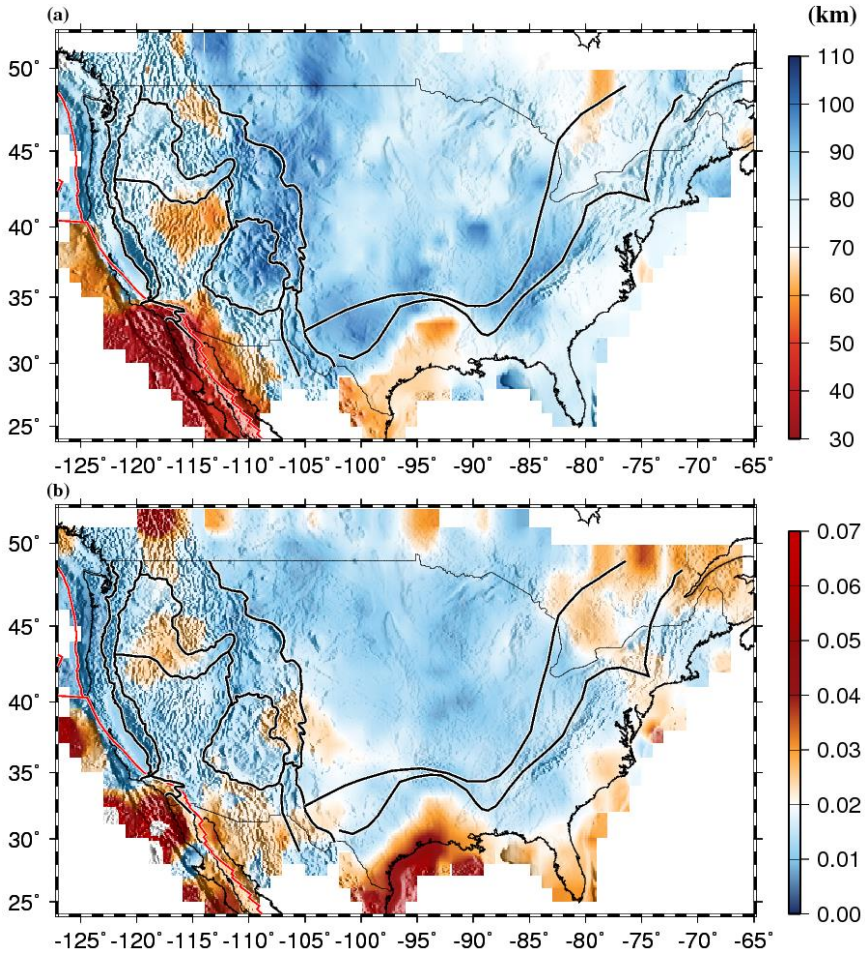

Figure 3. (a) Resulting depth distribution of the negative velocity discontinuity. (b) Distribution of stacking amplitudes (relative to that of the direct S-wave) for the NVD.

2. DATA AND METHODS

The broadband seismograms used in the study are obtained from the Incorporated Research Institutions for Seismology (IRIS) Data Management Center (DMC). A total of 3,594 stations contributed to the dataset, including 1,667 TA stations which sample the study area with an ~70 km interval. The seismograms are recorded within a duration of up to 28 years, from January 1988 to January 2016, during which all the USArray TA stations have finished their recording in the study area (125°W - 65°W and 25°N -50°N). The cutoff magnitude (Mc) for data requesting is calculated using $Mc = 5.2 + (\Delta - 30)/(180.0 – 30.0) – D/700.0$, where Δ is the epicentral distance in degree which is between 60° and 85° for the study, and D is the focal depth in km (Liu and Gao, 2010). The requested seismograms are then band-pass filtered in the frequency band of 0.06-0.6 Hz. Those with direct S-wave signal-to-noise ratio of 1.5 or greater on the radial component are selected to compute SRFs. The three-component ZNE (vertical, N-S, E-W) seismograms are rotated to LQT (P, S_V, S_H) components on the basis of theoretical back-azimuth and incident angle (Farra and Vinnik, 2000). The L component is in the propagation direction of the incident S-wave, primarily containing Sp energy and nearly zero direct S-wave energy for horizontally layered homogeneous media. The Q component, which is perpendicular to the L component, contains significant direct S_V -wave energy that can partially convert to P-wave at sharp velocity discontinuities (Farra and Vinnik, 2000). The rotated seismograms are time-reversed so that the Sp wave arrives after the direct S-wave and the crustal multiples prior to the S-wave. Subsequently, the L component is time-domain deconvolved by the S signal on the Q

component to generate SRFs for the purpose of eliminating the influence of the source (Langston, 1979; Kumar et al., 2012). The arrival time of the Sp wave in the SRFs depends on the depth of the discontinuity, the velocities in the overlying layer, and the ray parameter of the direct S-wave, whereas its amplitude is proportional to the velocity contrast across and the sharpness of the discontinuity.

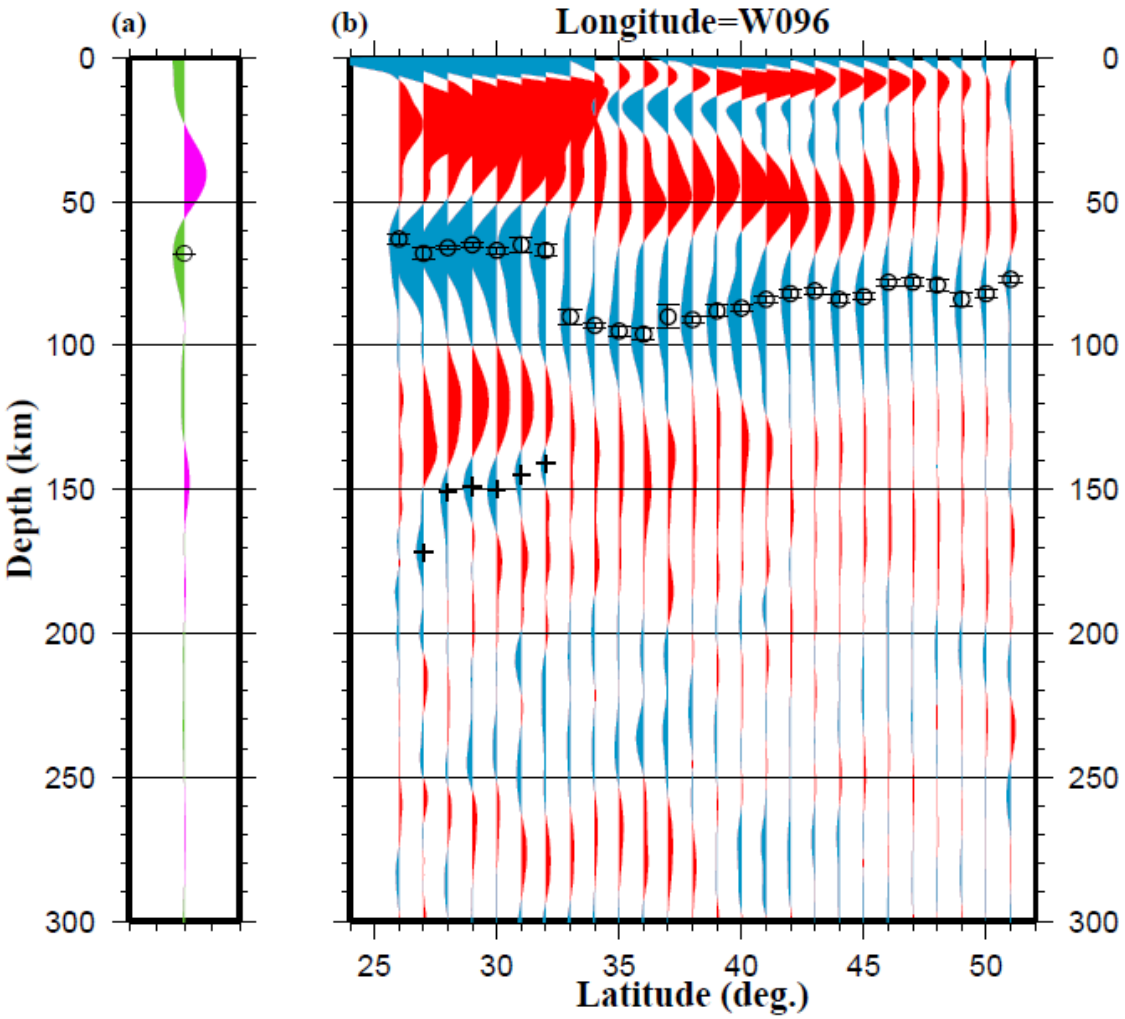

Figure 4. (a) Depth series from CORE synthetic seismograms. (b) Observed depth series along an N-S profile following the 96◦ W longitudinal line. The circles in the depth range of 60-100 km mark the NVD, and the pluses at the southern part of the profile indicate a negative arrival possibly representing the LAB beneath the Texas Coastal Plain.

The procedure to moveout correct and stack the SRFs is similar to the one that Gao and Liu (2014) used for imaging the mantle transition zone discontinuities across the contiguous U.S., and is briefly described below. To remove the influence of the ray parameter on the arrival times, moveout correction is then applied prior to CCP stacking to the SRFs using (Sheriff and Geldart, 1982; Dueker and Sheehan, 1997)

$$T_{Sp} - T_S = \int_{-h}^{0} [\sqrt{(V_s(z)^{-2} - p^2} - \sqrt{V_p(z)^{-2} - p^2}]dz, \qquad (1)$$

where p is the S-wave ray parameter, h is the depth of the candidate discontinuity which ranges from 0 to 300 km with an interval of 1 km, Vp(z) and Vs(z) are P and S-wave velocities, respectively, at depth z which are taken as the same as those in the IASP91 Earth model (Kennett and Engdahl, 1991). The SRFs are grouped into 2°-radius circular bins according to the location of the ray-piercing points computed based on the IASP91 Earth model. The distance between the center of neighboring bins is 1°. The SRFs in each of the bins are then moveout-corrected according to Eq. (1) and stacked to form a depth series with a vertical resolution of 1 km. To ensure reliability, bins with less than 50 SRFs are not used. The standard deviation of the resulting NVD depth is obtained through bootstrap resampling with 10 iterations. While a higher number of iterations can lead to more accurately determined mean and SD, the large number of SRFs involved in the computation requires about a week-long computation time for each iteration under today's CPU clock rate and especially the input/output rate of the storage device. More importantly, the NVD arrival for the vast majority of the bins is unambiguously identified (Figs. 2 and S1), and therefore increasing the number of bootstrap iterations would unlikely lead to significantly different results.

3. RESULTS

Totally 284,121 SRFs from 5,952 teleseismic events are used in the study. The number of SRFs per bin varies from 63 to 40,852 (Fig. 1). In comparison, the number of SRFs used by Hansen et al. (2015) for the central and western U.S. is 41,200, and that by Kumar et al. (2012) for the contiguous U.S. is 35,085. The edges of the study area are sampled by fewer SRFs, resulting in lower reliability than the interior. Fig. 2 shows examples of E-W cross-sections, and all the cross-sections with an interval of 1° can be found in Fig. S1, in which an NVD is observed corresponding to a robust negative arrival at the depth range of 30-110 km virtually in all the bins.

The depths of the NVD and the corresponding stacking amplitudes show systematic spatial variations, with mean values of 79 ± 13 km and 0.018 ± 0.009 over the study area, respectively (Fig. 3). In the following, these values are referred to as normal values. The tectonically active western U.S. west of the Rocky Mountains, the Colorado Plateau, and the Rio Grande Rift is dominated by shallow (30-90 km) and spatially varying NVD depths, which are in agreement with most previous SRF studies (Kumar et al., 2012; Lekić and Fischer, 2014; Hansen et al., 2015). The Basin and Range Province and the area adjacent to the Gulf of California have the smallest depths (as low as ~30 km) and relatively high amplitude (> 0.02), which are consistent with the measurements of Reeves et al. (2015). The NVD beneath the Coast Ranges is the deepest and the corresponding amplitude is the smallest in the western U.S. (~90 km and ~0.01, respectively), both are comparable to those observed beneath the central U.S. NVD

depths and amplitudes that are similar to the average over the study area are also found beneath the Columbia Plateau.

The Rocky Mountains and the neighboring Colorado Plateau are characterized by the deepest NVD in the whole study area, with a mean value of 95 ± 3 km. This is in agreement with the results of Levander and Miller (2012) who reported a mean of ~100 km. They are also consistent with the measurements of Kumar et al. (2012) and Hansen et al. (2015) for this study. The stacking amplitude in this area shows variable spatial distributions from 0.01 to 0.03.

The central U.S. demonstrates NVD depths ranging from 73 to 108 km, with an average of 87 ± 6 km. The depths of the NVD in the area have small spatial undulations, except for a few isolated areas such as the Llano Plateau in north-central Texas and the Southern Illinois Basin. The NVD depths are consistent with the measurements of Kumar et al. (2012), but are shallower than the results of Hansen et al. (2015), which show NVD depths of more than 160 km. Stacking amplitudes that are about half of those beneath the western U.S. are found in this area.

Anomalously shallow NVD depths and high stacking amplitudes are observed beneath the Texas-Louisiana Gulf Coastal Plain, in a coast-parallel band of about 200 km wide. The depths and amplitudes are spatially consistent within this band with a mean value of 63 ± 5 km and 0.030 ± 0.002, respectively. The NVD depth is significantly shallower than the ~110 km found by previous studies (Kumar et al., 2012; Hansen et al., 2015).

Slightly shallower than normal depths are revealed beneath the Grenville and Appalachian provinces of the eastern U.S., as well as the northeastern corner of the

central U.S. The depths range from 61-92 km, with an average of 76 ± 5 km. The NVD depths are consistent with SRF results obtained at isolated stations in the eastern U.S. (Rychert et al., 2007; Abt et al., 2010). The amplitudes in this region are in the range of 0.01-0.03 with an average of 0.023 ± 0.005, and are comparable to those in the western U.S.

The above depths were estimated based on the 1-D IASP91 Earth model and therefore the NVD depths are apparent rather than true depths. The uncertainty due to velocity perturbation in the depths can be estimated using Equation (2) in Gao and Liu (2014). For areas with a shallow NVD in the western and eastern U.S., under the assumption that there is a mean Vs anomaly of −5% for the layer above the NVD (Schaeffer and Lebedev, 2014), an apparent depth of 60 km, and a Vs and Vp relative velocity anomaly ratio of 2.0 (Gao and Liu, 2014), the estimated true depth is about 55 km. Similarly, for the central U.S., when the corresponding values of +4%, 90 km, and 1.8 are used, the estimated true depth is 96 km. The conclusion from the estimates is that in spite of the differences in the spatial distribution of the velocities in previous seismic tomography studies and in the Vs and Vp anomaly ratio, there is a possible bias in the estimated apparent depths of about 5 km. However, the contrast of the NVD depths between the central U.S. and the surrounding areas would be even more obvious in the corrected depths.

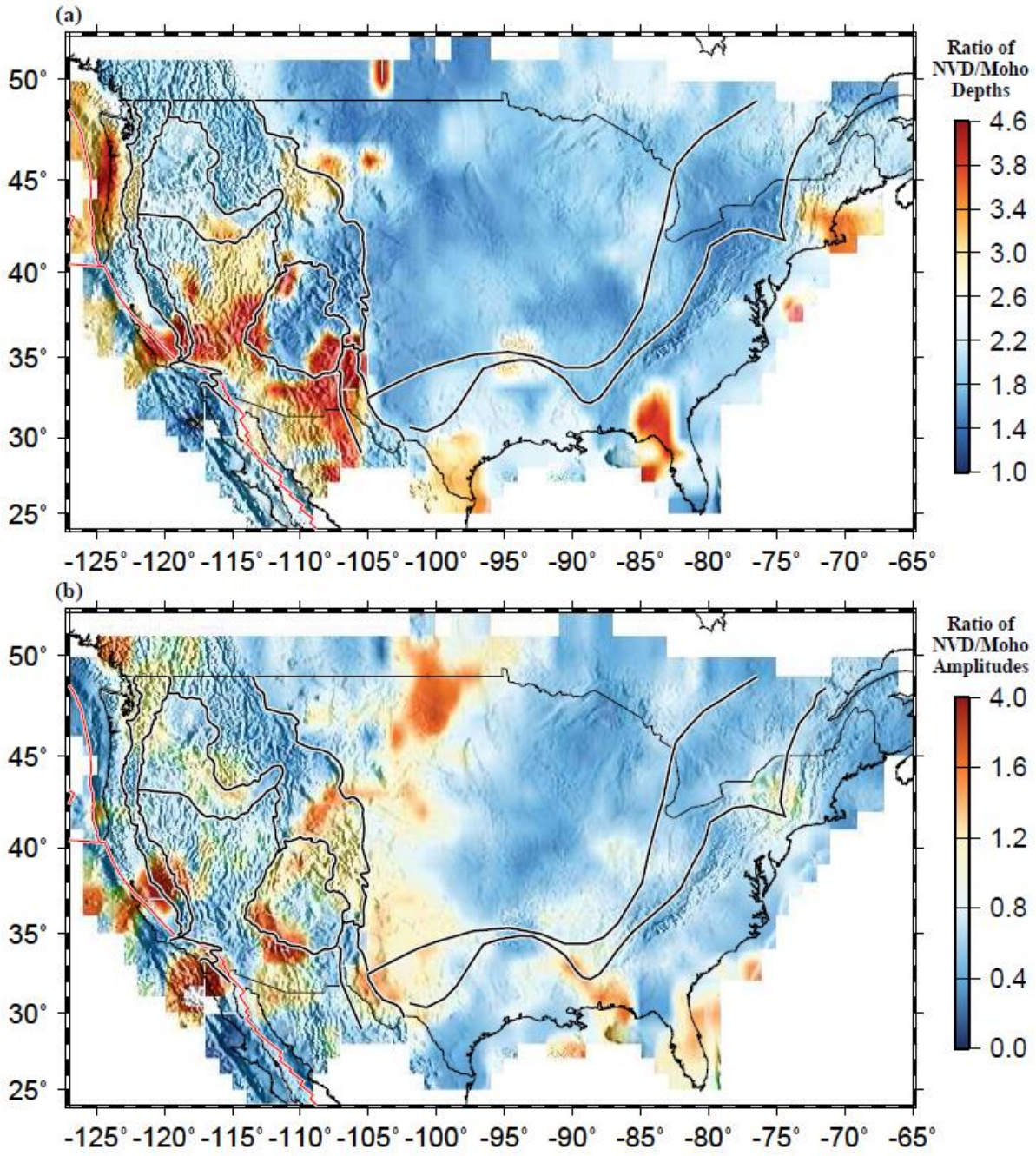

Figure 5. (a) Ratio of the depths of the observed NVD and the Moho. (b) Ratio of stacking amplitudes corresponding to the NVD and the Moho.

4. DISCUSSION

4.1. SYNTHETIC TEST

Due to the strong velocity increase (about 24% for Vp and 19% for Vs) across the Moho (Kennett and Engdahl, 1991), there is a robust positive arrival in the resulting SRFs corresponding to the Moho. With limited band width, a side-lobe may exist and could be misidentified as the NVD (e.g., Li et al., 2007; Kumar et al., 2012; Hansen et al., 2015). To investigate this possibility, we produce about 2,000 synthetic seismograms with randomly assigned focal parameters (focal depth, epicentral distance, and focal mechanisms) using the Complete Ordered Ray Expansion (CORE) suite of programs (Clarke, 1993). The input 1-D model includes a 35 km thick crust, the 410 and 660 km discontinuities, and the core-mantle boundary. The velocities and densities are the same as those in the IASP91 Earth model. The synthetic seismograms are then processed and stacked using exactly the same procedures as those used for the real data.

The resulting depth series produced using the synthetic SRFs (Fig. 4a) indeed possesses a negative arrival beneath the positive one corresponding to the Moho. However, comparing with the depth series created using the observed data (Fig. 4b), several differences can be observed. First, on the synthetic result, the ratio between the depth of the negative arrival beneath the Moho and the depth of the Moho (Fig. S2) is about 1.8, while it varies systematically from 1.0 to 4.6 across the study area (Fig. 5a). Even when possible lateral variations in crustal velocities are considered, it is unlikely that the depth of the Moho side-lobe can display such variability. Second, the ratio between the amplitudes of the sub-Moho negative arrival and the Moho arrival (Fig. S2)

is about 0.4 on the synthetic trace, while that for the observed data is mostly greater than 0.4 and can be as large as 4.0 (Fig. 5b). Third, while the two side-lobes on the synthetic trace are symmetric with regard to the peak of the Moho arrival, the two negative arrivals on most of the observed traces are asymmetric, with the lower one being significantly more separated from the Moho arrival (Fig. 4). Therefore, the result of the synthetic test is inconsistent with the possibility that the NVD is a side-lobe of the Moho arrival on the SRFs. Instead, it represents a real negative discontinuity in the upper mantle.

4.2. A SHALLOW AND SHARP LITHOSPHERE-ASTHENOSPHERE TRANSITIONAL LAYER IN THE WESTERN U.S.

The mean depth (69 ± 17 km) of the NVD observed beneath the western U.S. is comparable to the depth of the bottom of the rigid lithosphere revealed from seismic surface wave tomography (Schaeffer and Lebedev, 2014) and the depth of the LAB inferred from mantle xenolith data (Mareschal and Jaupart, 2004). Therefore, similar to previous SRF studies (e.g., Kumar et al., 2012; Lekić and Fischer, 2014; Hansen et al., 2015), we consider this discontinuity to be the sharp lithosphere-asthenosphere transitional layer (LATL; Figs. 6 and S3) which is commonly referred to as the LAB in previous studies. This interpretation of the NVD is consistent with the inferred anomalously high temperature of 1200°C at the depth of about 80 km beneath the western U.S. (Hansen et al., 2015).

In the area adjacent to the Gulf of California, the depth of the LATL is the shallowest (30-50 km) in the entire study area, and the crustal thickness varies from 20 to 25 km (Yan and Clayton, 2007; Zhu and Kanamori, 2000). The thinning of both the crust and sub-crustal lithosphere beneath the Gulf of California and adjacent areas is consistent

with the hypothesis of strain-localization-induced lithospheric thinning, probably originating from the clockwise rotation of the Transverse Range (Reeves et al., 2015).

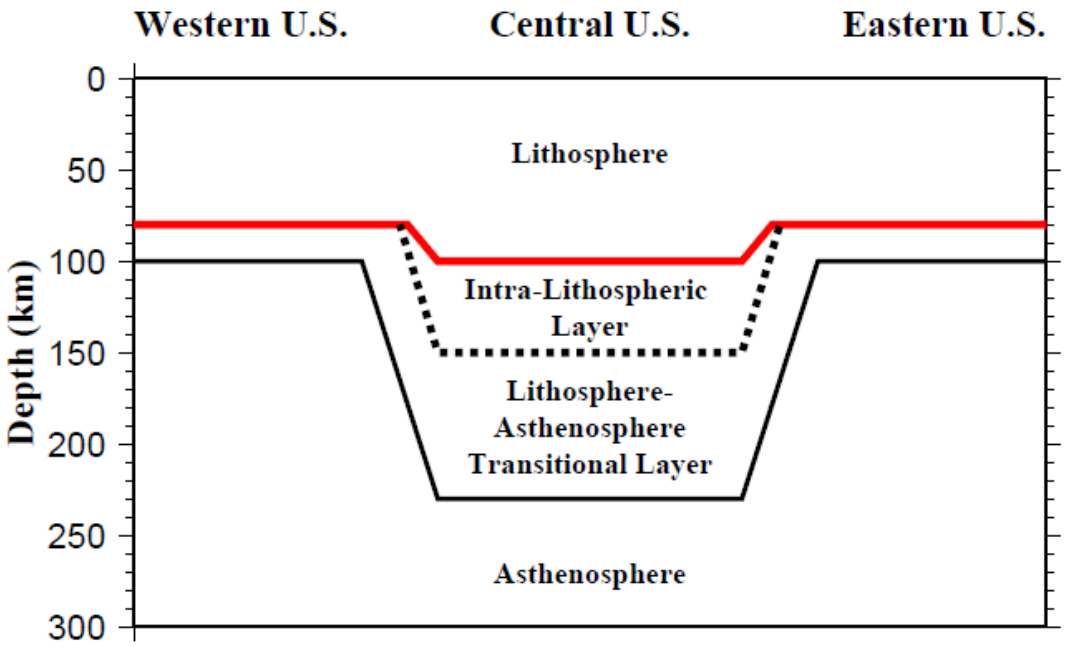

Figure 6. A schematic model illustrating the stratification of the lithosphere along an E-W profile across the study area. The red line is the SRF-detected boundary.

Another area with thin lithosphere (~60 km) in the western U.S. is the Basin and Range Province (BRP), which is characterized by crustal thinning as well. For the BRP, there are two possible mechanisms contributing to the thinning of the lithosphere, including removal of the lower part of the lithosphere by the Farallon flat-lying subduction (Humphreys, 1995; Cox et al., 2016), and middle to late Cenozoic continental extension (Wernicke and Snow, 1998; Lekić and Fischer, 2014). With an average crustal thickness of 25 km and 50 km beneath the BRP and the Colorado Plateau, respectively, the crustal stretch rate of the BRP is 60-100% based on previous studies (Bashir et al., 2011). Comparing with our observations of lithospheric thickness beneath the BRP (50-

70 km) and the neighboring Colorado Plateau (90-110 km), the amount of thinning of the sub-lithosphere is approximately proportional to that of the crust if we assume that the pre-stretching lithospheric thickness was comparable beneath the Plateau and surrounding areas. Therefore, uniform lateral stretching of the entire lithosphere seems to be a viable cause of the observed lithospheric thinning.

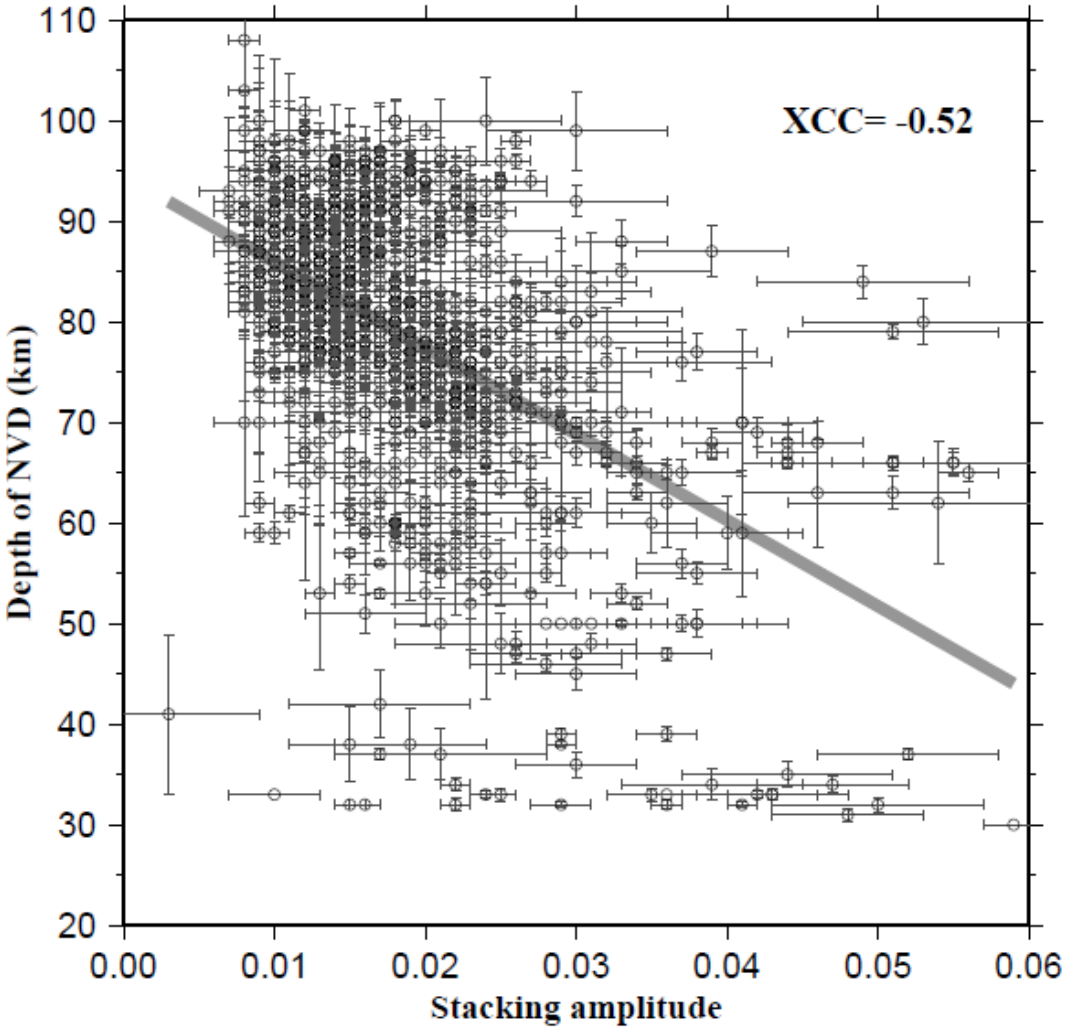

Figure 7. Depths of the NVD plotted against the corresponding stacking amplitudes for stations in the Western U.S. XCC: cross correlation coefficient.

The thickest lithosphere and smallest stacking amplitudes in the western U.S. are observed beneath the Cascade Range-Sierra Nevada, which is mostly located above the subducted Juan De Fuca slab. The reduced velocity contrast across the LATL beneath this area, as reflected by the small stacking amplitudes, might be caused by partial melting within the lithospheric mantle induced by the hydrous oceanic slab (Walowski et al., 2016). Dehydration reactions have been recognized by previous studies (Walowski et al., 2016), and flux melting of the crust of the Juan De Fuca slab may have migrated into the overlying mantle of the North American plate, resulting in melting in the lower lithosphere, which in turn may reduce mantle velocities and result in the observed small stacking amplitudes.

In general, beneath the western U.S., areas with thin lithosphere possess large stacking amplitudes and vice versa (Fig. 7). The cross correlation coefficient is -0.55, indicating the robust negative relationship between the thickness and amplitude. One of the simplest explanations for this relationship is a higher degree of partial melting in the top-most layer of the asthenosphere beneath thinner lithosphere, leading to a greater velocity contrast between the lithosphere and asthenosphere. Under the assumption that the bottom of the lithosphere is a constant temperature interface, the lower pressure corresponding to a thinner lithosphere leads to a higher degree of partial melting (e.g., Ganguly, 2005). Experimental and modeling studies suggest that melting can be induced by the presence of volatiles (Green et al., 2010) and by a dramatic reduction in water solubility of aluminous orthopyroxene (Mierdel et al., 2007).

4.3. AN INTRA-LITHOSPHERIC LOW-VELOCITY LAYER BENEATH THE CENTRAL U.S.

Most seismic surface wave tomography studies suggest that beneath the cratonic region of the central U.S., the thickness of the lithosphere is about 250 km and can be further divided into various sub-layers (Bedle and van der Lee, 2009; Yuan and Romanowicz, 2010; Schaeffer and Lebedev, 2014). Therefore, the NVD observed at the average depth of 87 ± 6 km beneath this area is a mid-lithospheric discontinuity. Combined with previous results of mantle temperature (Hansen et al., 2015), shear wave velocity (Abt et al., 2010; Yuan and Romanowicz, 2010), with the weaker amplitude corresponding to the NVD relative to that of the western U.S. obtained in this study (Fig. 3b), this discontinuity may represent the top boundary of a 40-60 km thick low-velocity intra-lithospheric layer (ILL). This interpretation is consistent with the lithospheric layering model obtained from joint inversion of long and short period seismic data (Calò et al., 2016), which detected double MLDs at depths of about 100-130 and 150-170 km, indicating the top and bottom of a low-velocity ILL. The 70-km-wide thermal root is a gradual instead of sharp LATL between the bottom of the ILL and the underlain asthenosphere (Fig. 6).

Several formation mechanisms have been proposed for this sharp MLD, including 1) high geothermal gradients or presence of partial melt (Yuan and Romanowicz, 2010; Kumar et al., 2012); 2) variation in the geometry of seismic anisotropy, from diffusion/superplastic to dislocation creep (Wirth and Long, 2014; Ford et al., 2016); and 3) compositional variation caused by metasomatism or crystallized melts, e.g., volatile, chemical depletion or low-velocity minerals such as amphibole and phlogopite (Griffin et al., 2004; Foster et al., 2014; Hansen et al., 2015; Hopper and Fischer, 2015). In depth

discussions of the above mechanisms can be found in Hansen et al. (2015), who conclude that the ILL is most likely a compositionally distinct layer that is rich in phlogopite.

4.4. LITHOSPHERIC EXTENSION IN THE TEXAS-LOUISIANA GULF COASTAL PLAIN

The Gulf Coastal Plain has undergone several complicated geological processes, such as collision, extension, and rifting (Evanzia et al., 2014). The shallow but strong NVD observed at the depth of ~60 km beneath this area can be interpreted as a low-velocity layer within the lithosphere (Ainsworth et al., 2014), similar to the central U.S. If we assume that the original depth of this interface is the same as that beneath the central U.S. (~100 km), a stretching (β) factor of about 1.7 is obtained. This is comparable to the average crustal stretching factor (e.g., Mickus et al., 2009) and suggests that the shallowing of the NVD is the consequence of lithospheric extension. An alternative explanation of the shallow NVD is that it is the result of an upward propagation of a metasomatic front associated with increased heat flow in areas with continental extension (Thibault et al., 1992; Hansen et al., 2015).

Beneath this area, another negative signal is observed at the depth of ~150 km (Fig. 4b). It is not seen on the synthetic trace (Fig. 4a) and thus is unlikely to be an artifact (which is possibly the case for the positive arrival above the negative one which appears on the synthetic trace at the depth of about 150 km). This discontinuity has also been observed by previous studies (Kumar et al., 2012; Ainsworth et al., 2014; Hansen et al., 2015) and could be interpreted as representing the bottom of the rigid lithosphere. Under the assumption that the pre-stretching lithosphere is similar to that beneath the central U.S. (~250 km), the β factor for the lithosphere is ~1.7, which is the same as the β

factor computed using the depth of the NVD. Note that relative to the western half of the Coastal Plain, the eastern part (east of 90°W) shows much smaller stretching.

4.5. LITHOSPHERIC MODIFICATION IN THE EASTERN U.S.

The depth and amplitude of the NVD beneath the eastern U.S. are similar to those observed beneath the tectonically active western U.S. Additionally, like for the western U.S., based on the similarities between the SRF-revealed and tomographically-determined depths, we consider the NVD to be representing a sharp LATL, as proposed by previous SRF studies (Rychert et al., 2007; Abt et al., 2010). Beneath the northeastern U.S., the LATL is notably shallower (~70 km) and the amplitude is higher (~0.03) than those of the neighboring regions (Fig. 3). In this area, a low-velocity anomaly at the base of the lithosphere, referred to as an indentation or Great Lakes mantle divot, has been suggested by seismic tomographic studies, and was regarded as the consequence of mantle plume accumulation (Bedle and van der Lee, 2009; Burdick et al., 2017). The observed thinning of the lithosphere (Fig. 3a) could be the result of lithosphere-plume interaction (Eaton and Frederiksen, 2007), and the increased velocity contrast between the bottom of the eroded lithosphere and the underlying mantle plume material can explain the observed high stacking amplitudes beneath this area (Fig. 3b).

5. CONCLUSIONS

A robust negative velocity discontinuity is pervasively detected in the contiguous U.S. in the depth range of 30-110 km in consecutive 2° circular bins using a high number of S receiver functions that is unprecedented for the study area. Beneath the extended crust of the western U.S. and the Gulf Coastal Plain and the eastern U.S., similarities between the depth of the this discontinuity and depths of the LAB revealed by seismic tomography and xenolith studies suggests that it represents the sharp transitional layer between the cold lithosphere and partially melt asthenosphere. In contrast, beneath the stable cratonic region of the central U.S., this discontinuity is most likely the sharp upper boundary of a chemically distinct layer probably formed by metasomatism in the ancient lithosphere. Further investigations are needed in order to understand the contrasting thickness of the LATL between the cratonic central U.S. and the adjacent tectonically younger areas.

An intriguing anti-correlation between the depth of the negative velocity discontinuity and the amplitude of the Sp wave is revealed for the western U.S. One of the simplest explanations for this relationship is that the top-most layer of the asthenosphere experiences more volatile-induced melting beneath thinner lithosphere. Uniform extension of the lithosphere in the Basin and Range Province and the Texas-Louisiana Gulf Coastal Plain can satisfactorily explain the observed thinning of the crust and the whole lithosphere. Finally, anomalously thin lithosphere and large stacking amplitudes observed beneath the northeastern U.S. may indicate erosion of the bottom of the lithosphere, probably by a passing mantle plume.

SUPPLEMENTARY INFORMATION

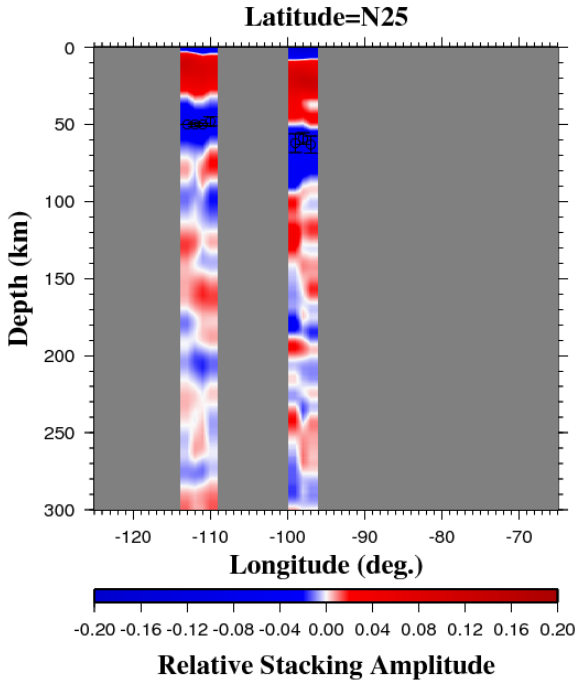

Figure S1a. E-W stacked S-to-P Receiver Function profiles along latitudinal line 25°N. Warm (cool) colors indicate velocity increase (decrease) with depth. The circles trace the Negative Velocity Discontinuity in the upper mantle.

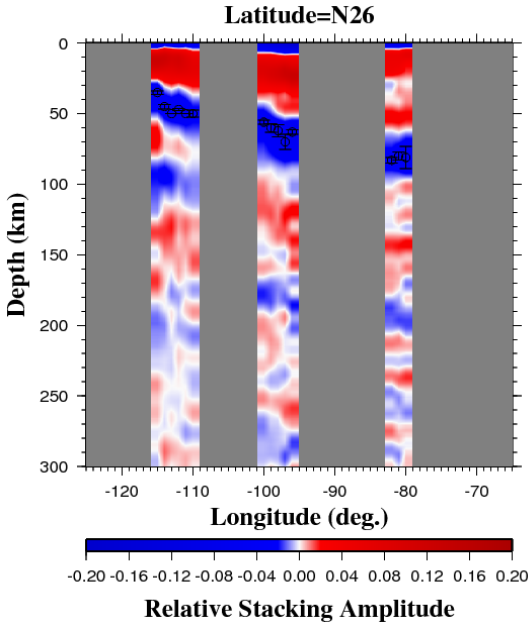

Figure S1b. Same as Figure S1a but for latitudinal line 26°N.

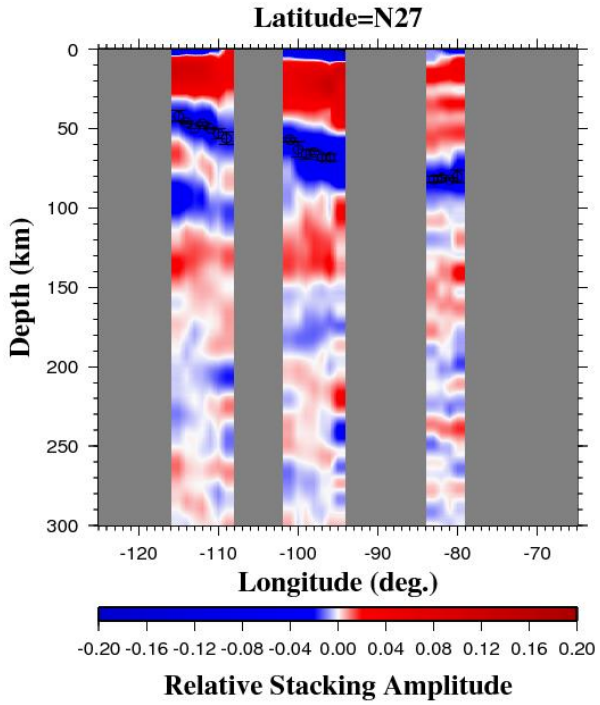

Figure S1c. Same as Figure S1a but for latitudinal line 27°N.

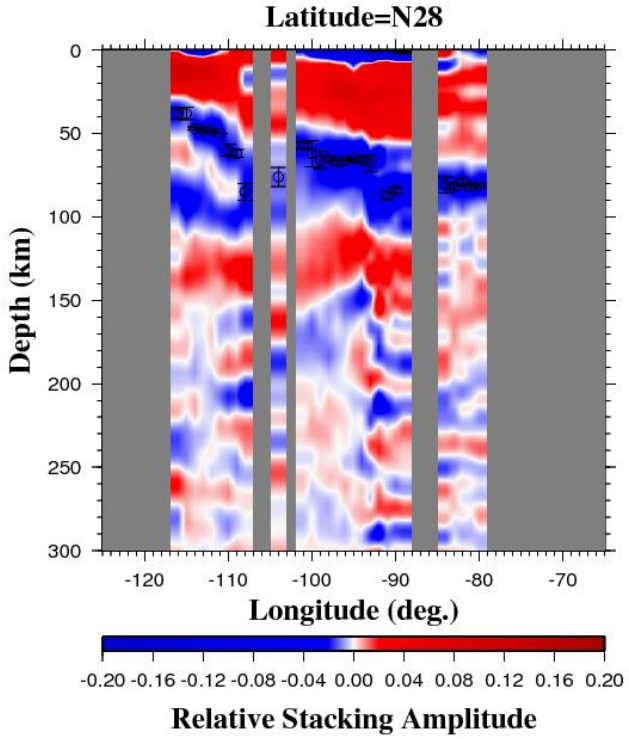

Figure S1d. Same as Figure S1a but for latitudinal line 28°N.

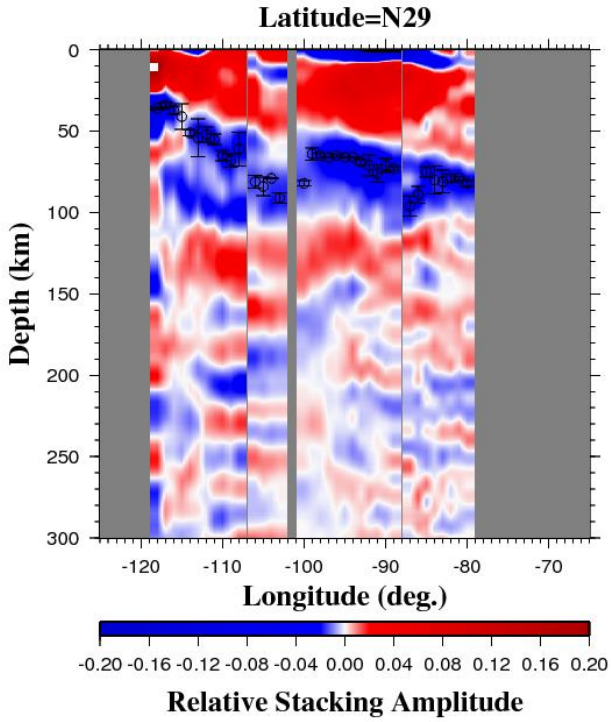

Figure S1e. Same as Figure S1a but for latitudinal line 29°N.

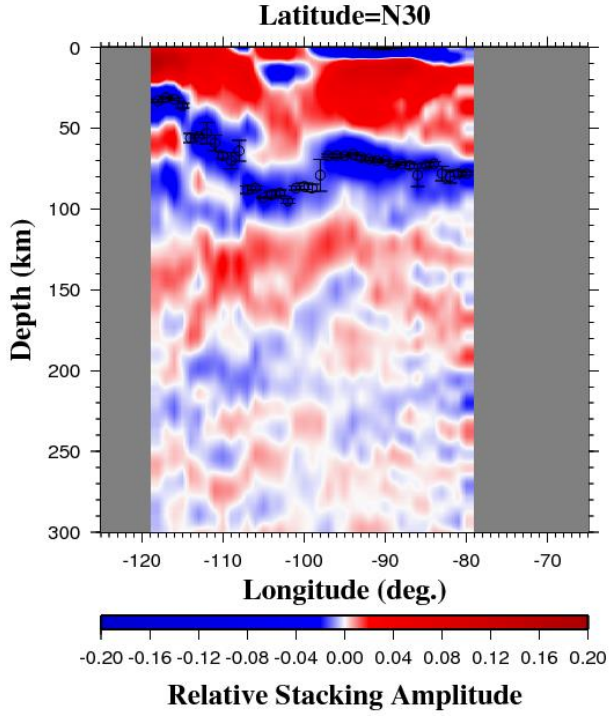

Figure S1f. Same as Figure S1a but for latitudinal line 30°N.

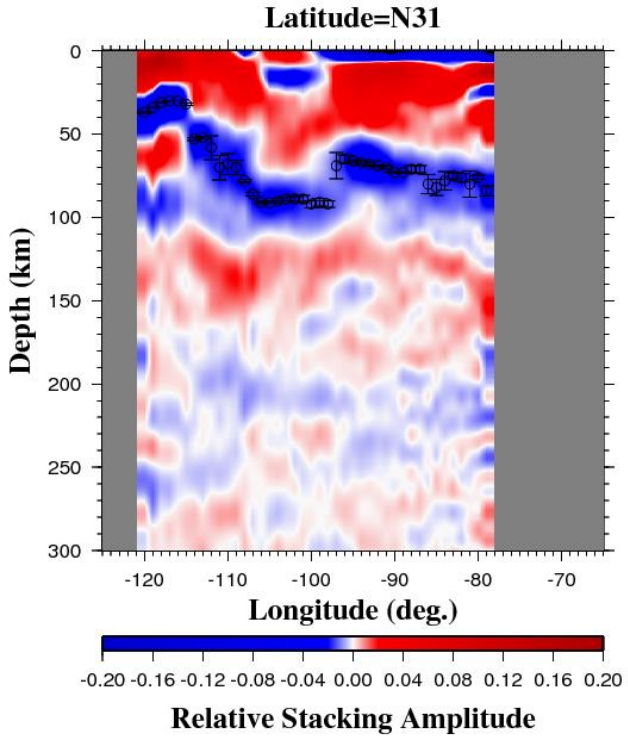

Figure S1g. Same as Figure S1a but for latitudinal line 31°N.

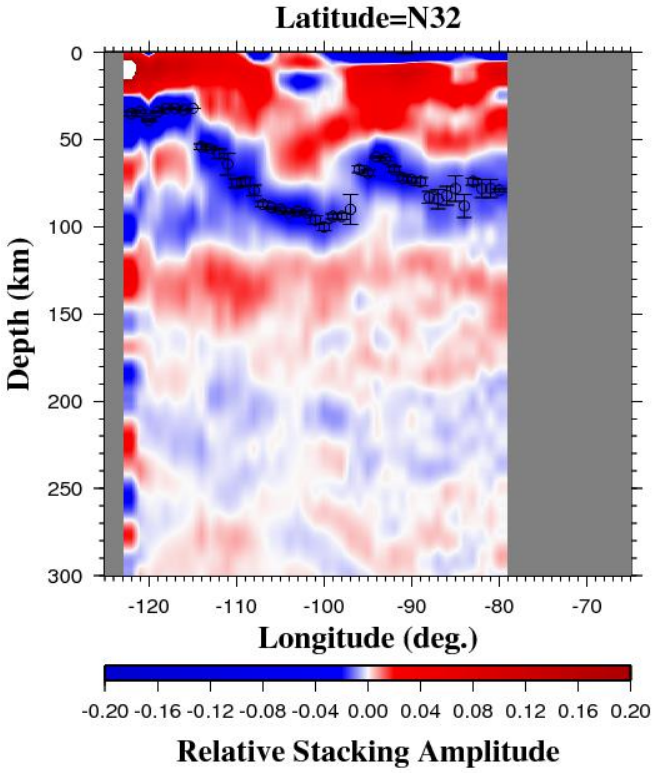

Figure S1h. Same as Figure S1a but for latitudinal line 32°N.

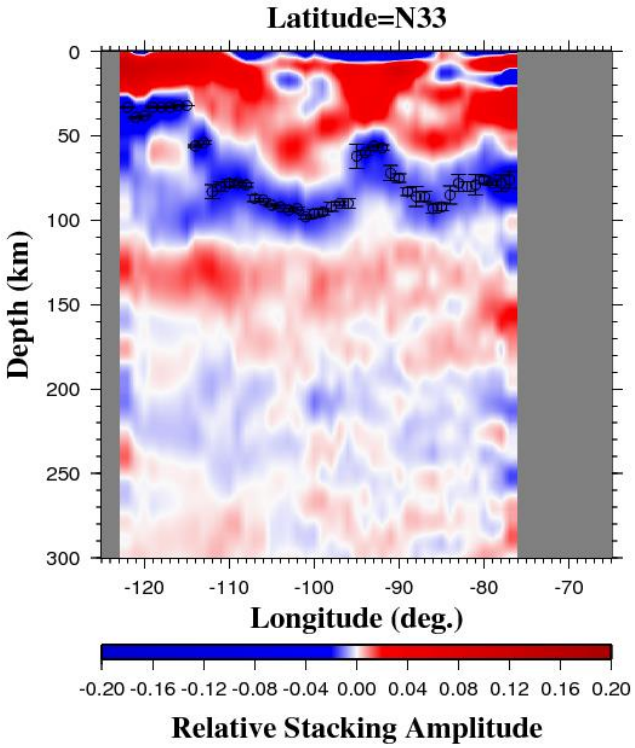

Figure S1i. Same as Figure S1a but for latitudinal line 33°N.

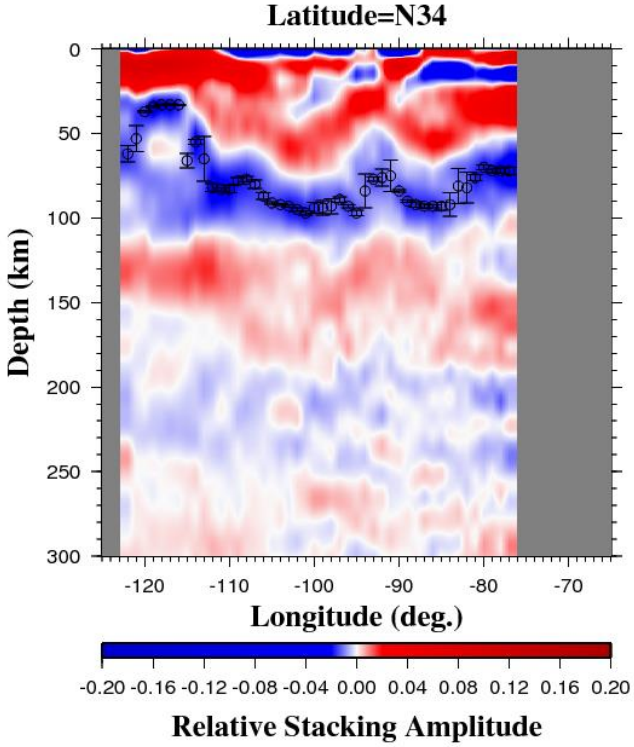

Figure S1j. Same as Figure S1a but for latitudinal line 34°N.

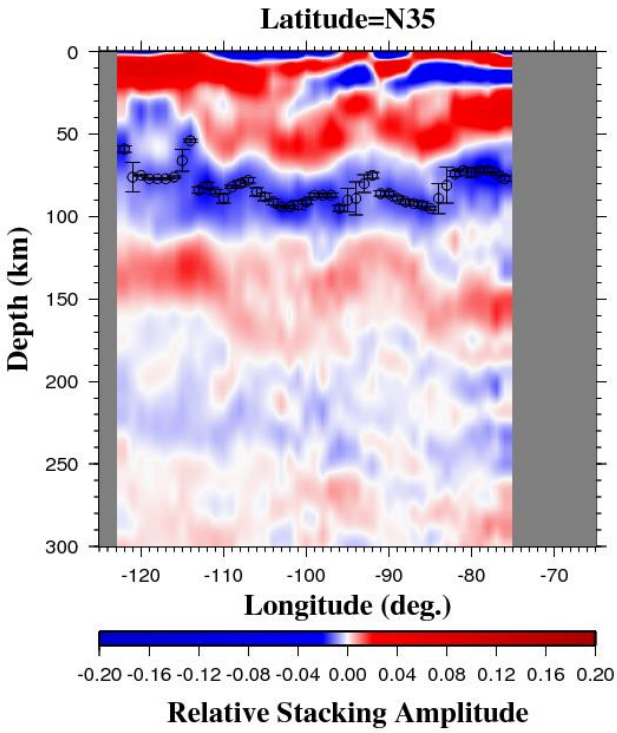

Figure S1k. Same as Figure S1a but for latitudinal line 35°N.

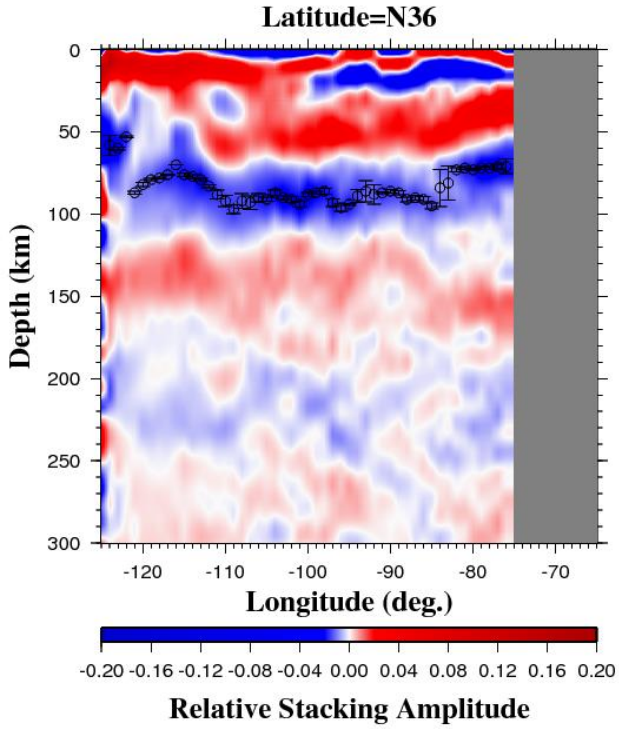

Figure S1l. Same as Figure S1a but for latitudinal line 36°N.

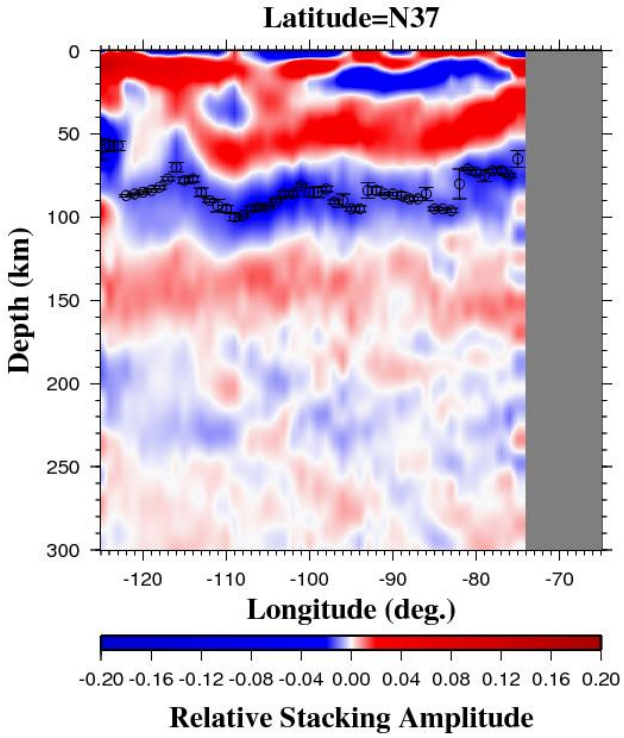

Figure S1m. Same as Figure S1a but for latitudinal line 37°N.

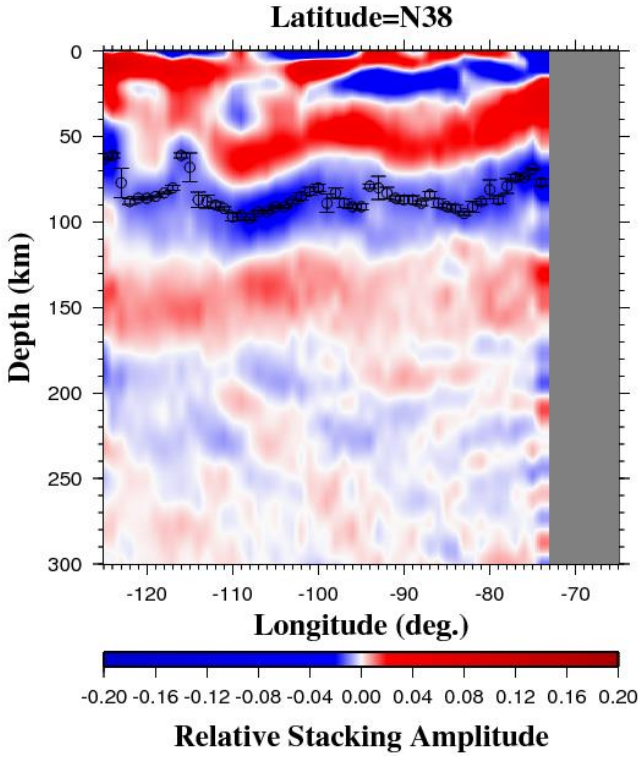

Figure S1n. Same as Figure S1a but for latitudinal line 38°N.

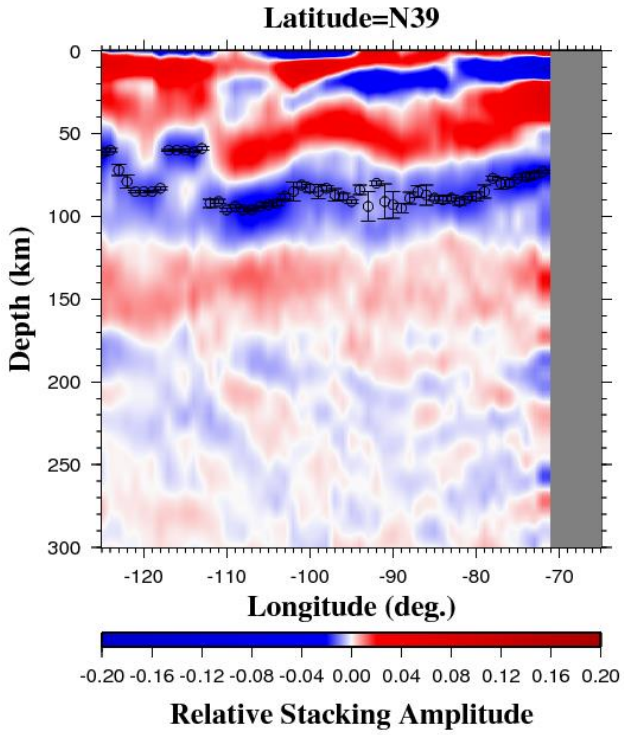

Figure S1o. Same as Figure S1a but for latitudinal line 39°N.

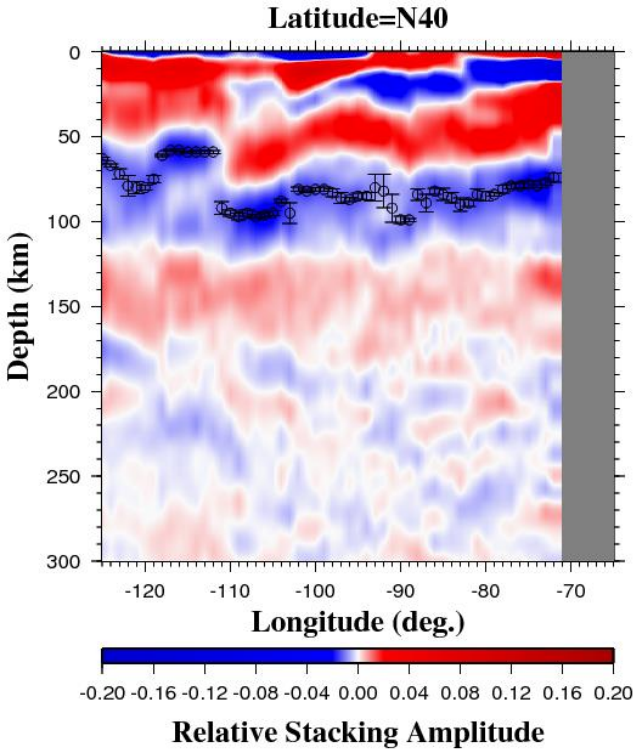

Figure S1p. Same as Figure S1a but for latitudinal line 40°N.

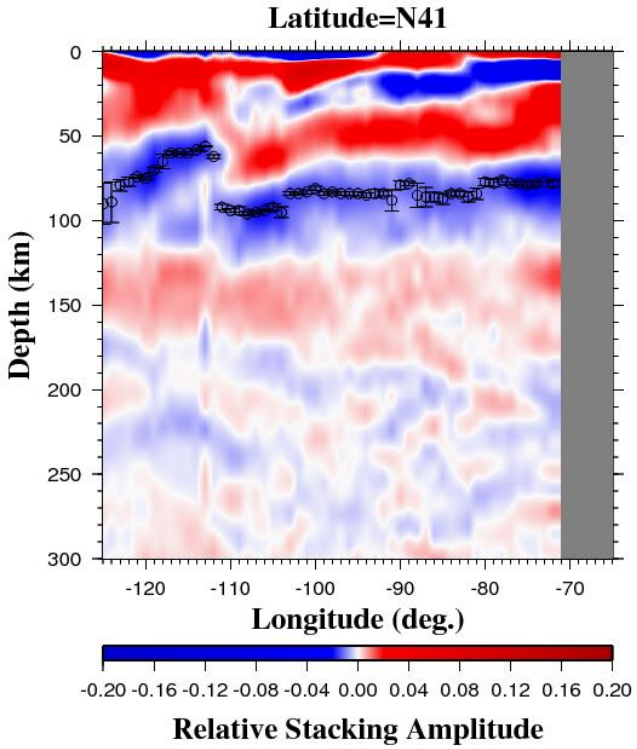

Figure S1q. Same as Figure S1a but for latitudinal line 41°N.

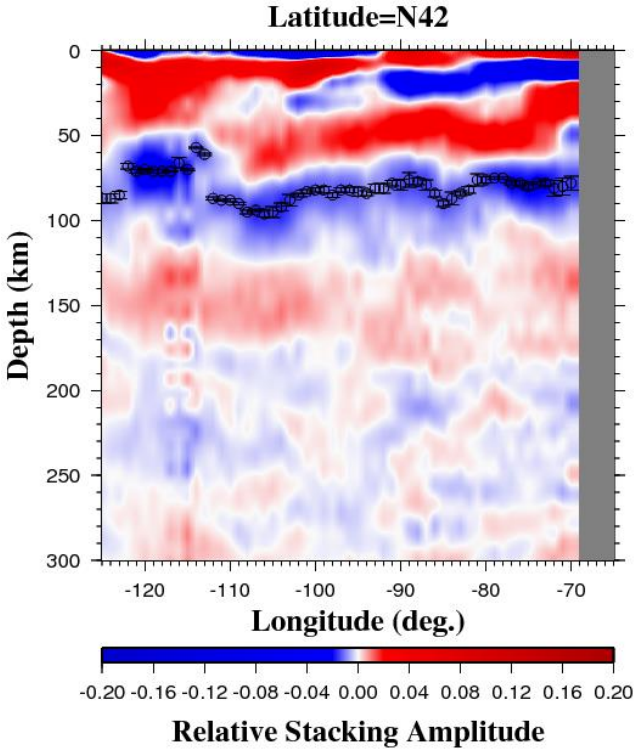

Figure S1r. Same as Figure S1a but for latitudinal line 42°N.

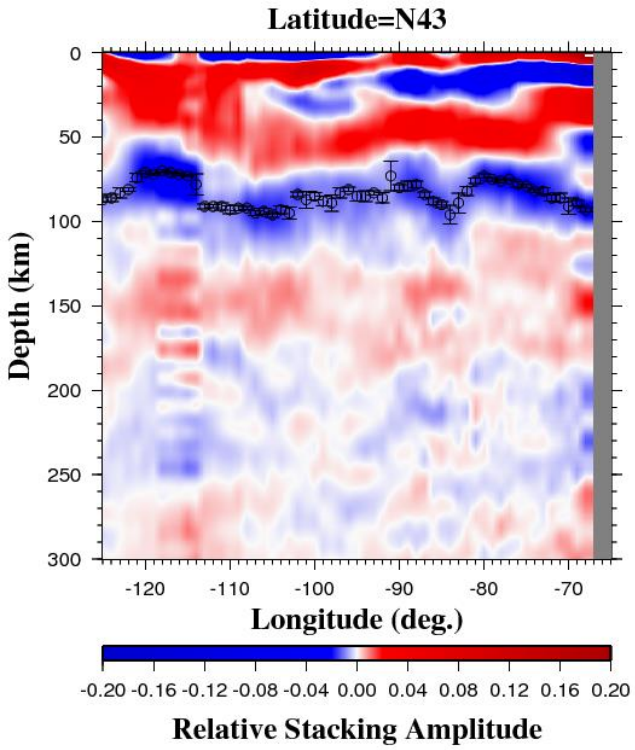

Figure S1s. Same as Figure S1a but for latitudinal line 43°N.

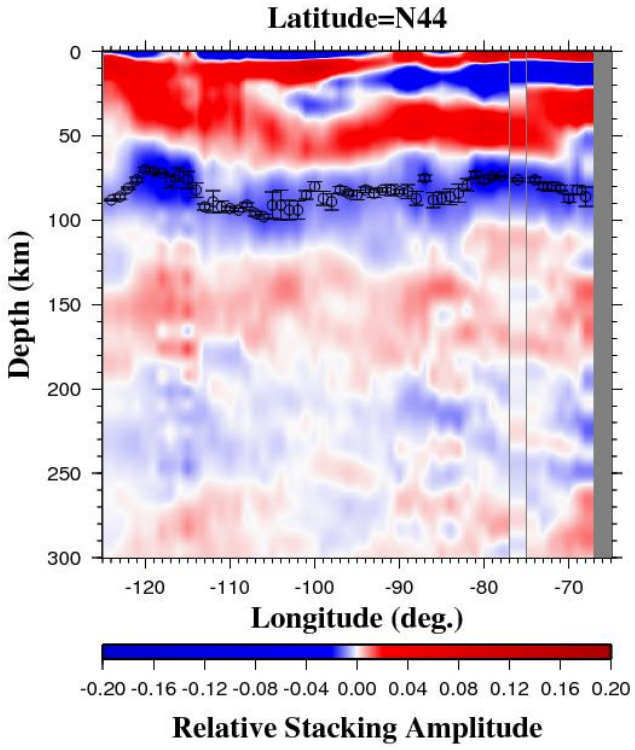

Figure S1t. Same as Figure S1a but for latitudinal line 44°N.

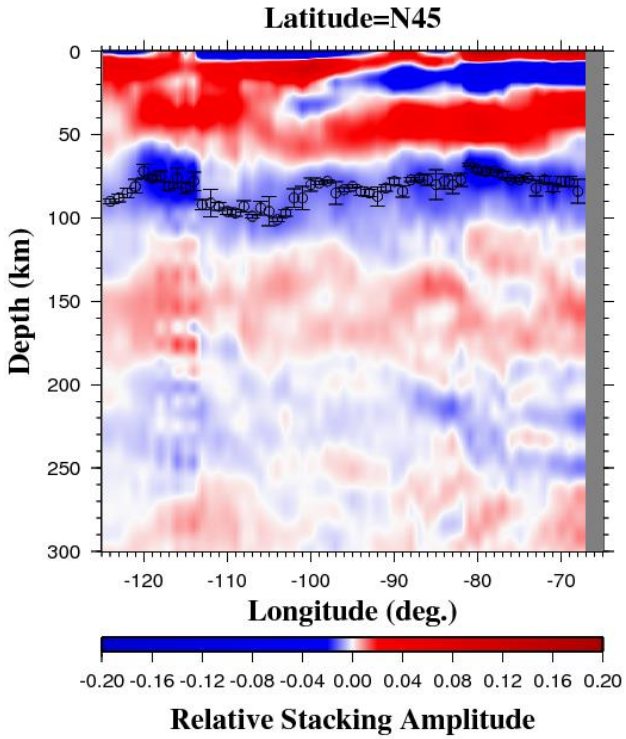

Figure S1u. Same as Figure S1a but for latitudinal line 45°N.

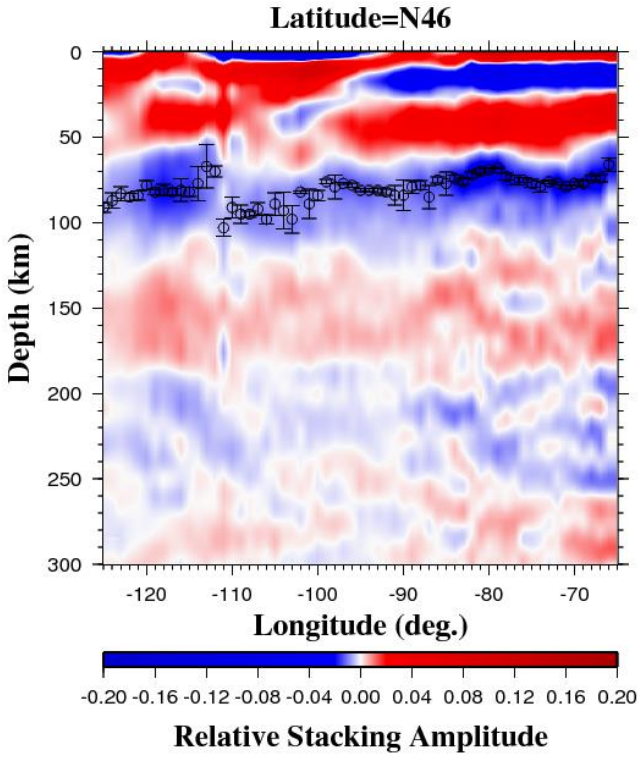

Figure S1v. Same as Figure S1a but for latitudinal line 46°N.

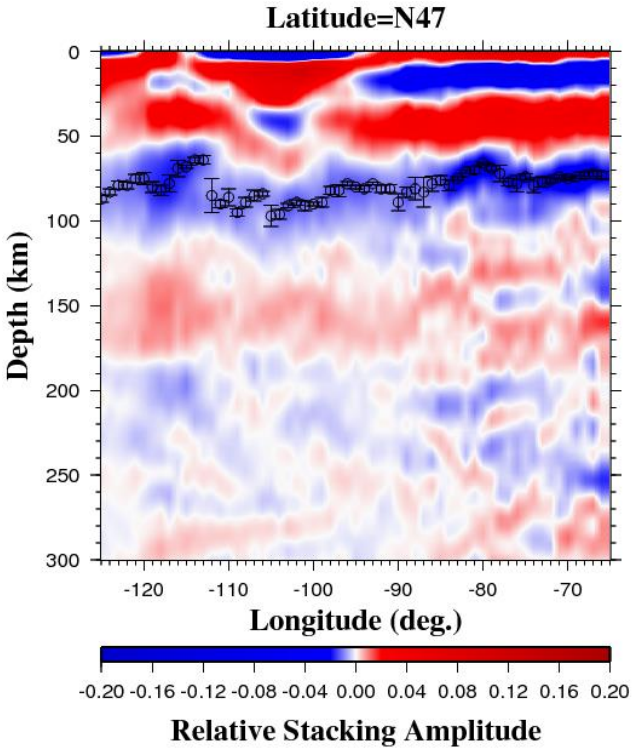

Figure S1w. Same as Figure S1a but for latitudinal line 47°N.

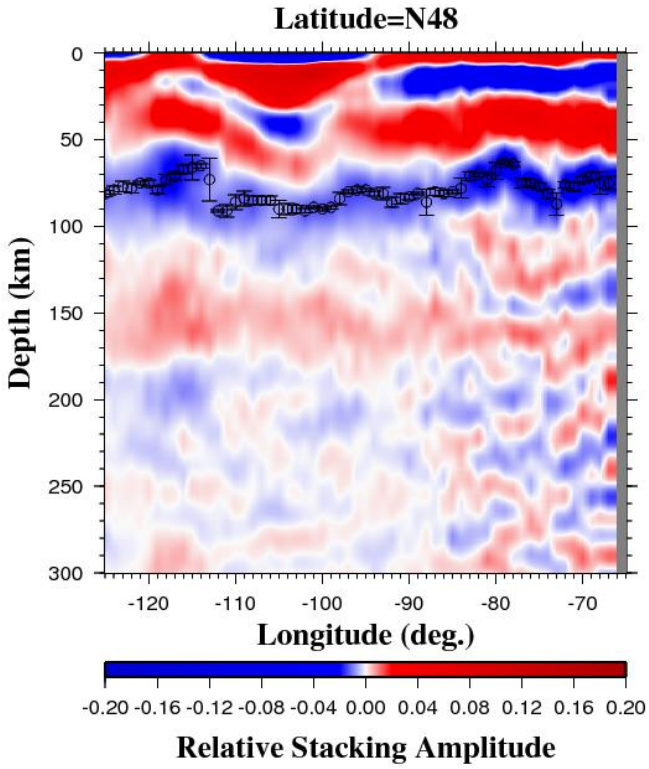

Figure S1x. Same as Figure S1a but for latitudinal line 48°N.

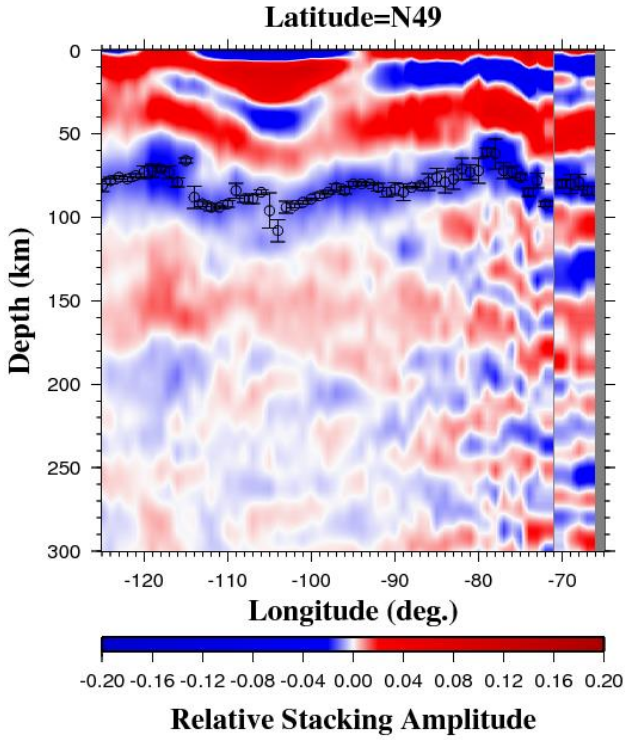

Figure S1y. Same as Figure S1a but for latitudinal line 49°N.

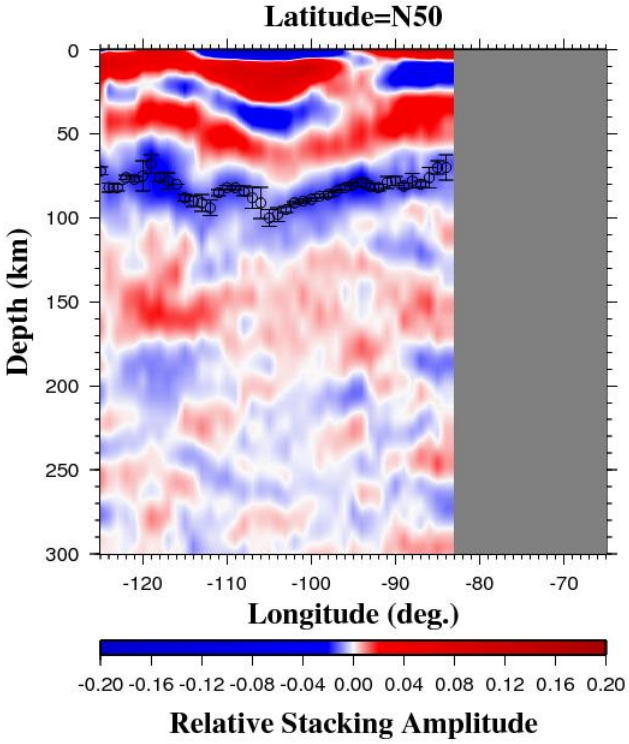

Figure S1z. Same as Figure S1a but for latitudinal line 50°N.

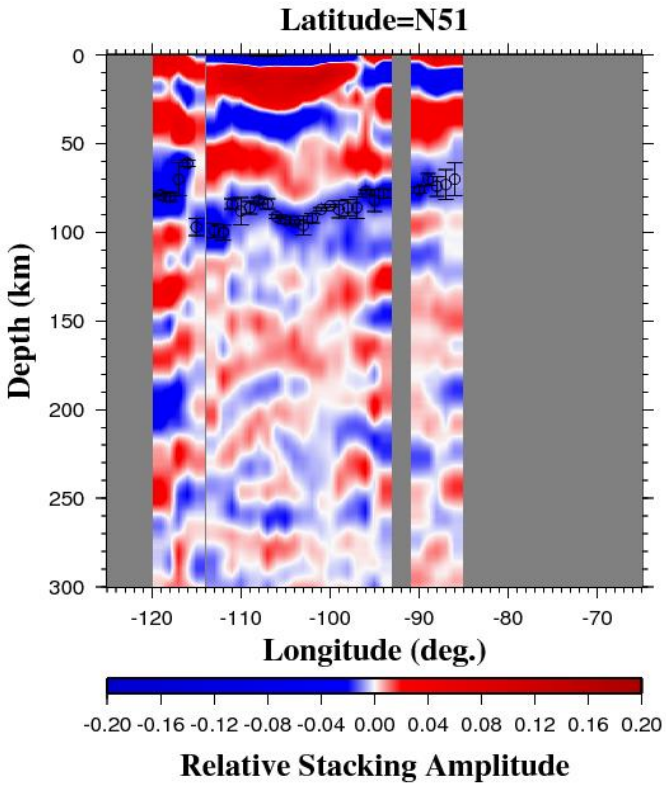

Figure S1aa. Same as Figure S1a but for latitudinal line 51°N.

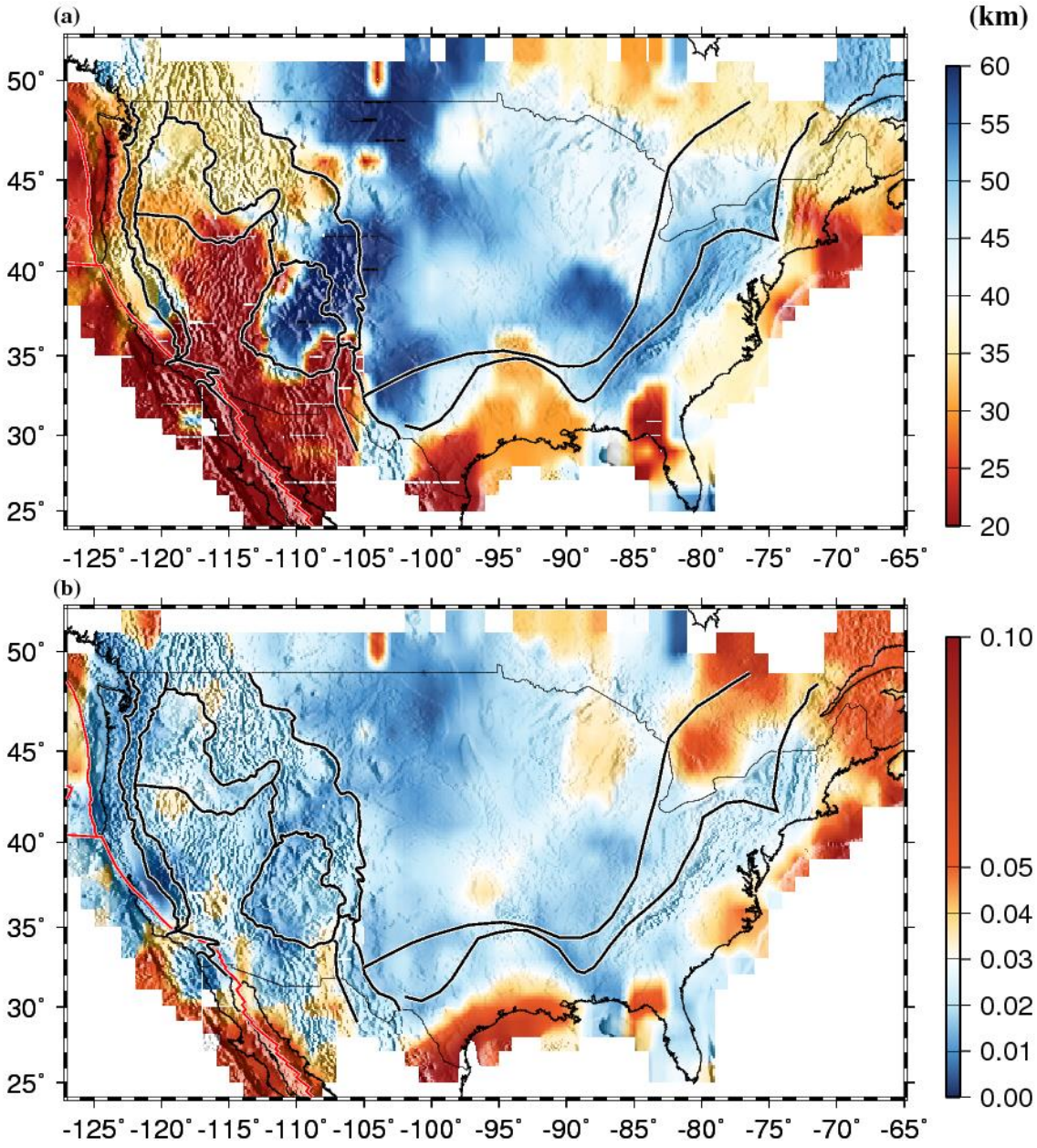

Figure S2. (a) Resulting depth distribution of the Moho. (b) Distribution of stacking amplitudes (relative to that of the direct S-wave) for the Moho.

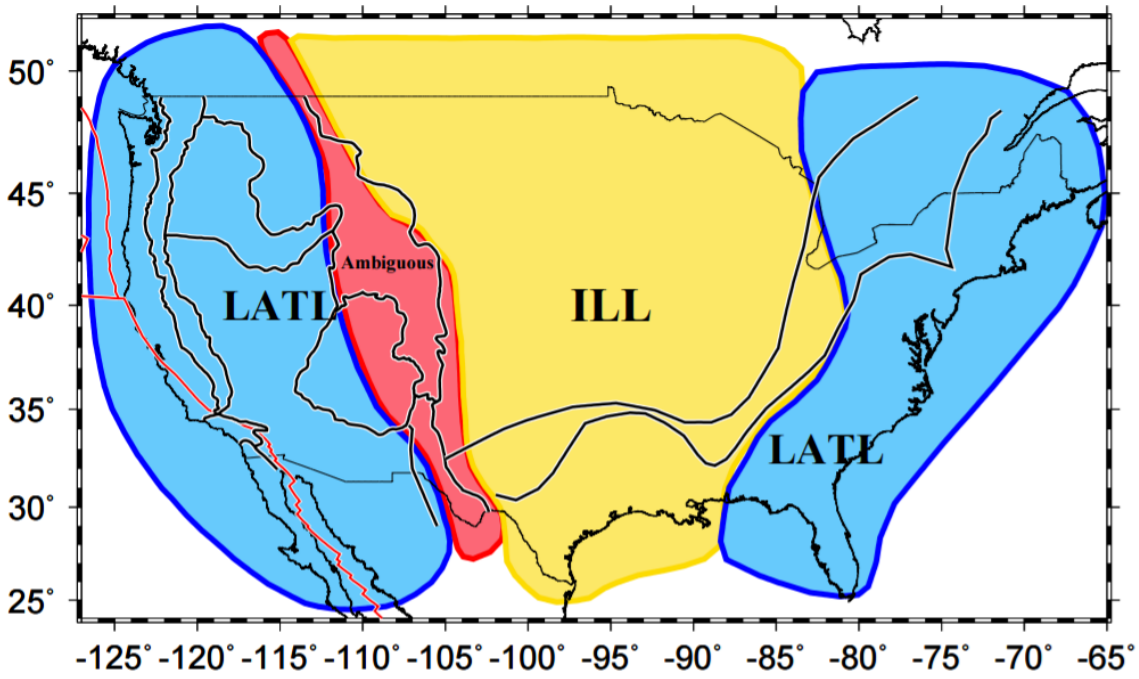

Figure S3. The approximate geographic distribution of the classification of the Negative Velocity Discontinuity.

REFERENCES

Abt, D. L., Fischer, K. M., French, S. W., Ford, H. A., Yuan, H., and B. Romanowicz (2010), North American lithospheric discontinuity structure imaged by Ps and Sp receiver functions, J. Geophys. Res. 115(B9), doi:10.1029/2009JB006914.

Ainsworth, R., Pulliam, J., Gurrola, H., and D. Evanzia (2014), Sp receiver function imaging of a passive margin: Transect across Texas's Gulf Coastal Plain, Earth Planet, Sci. Lett., 402, 138-147, doi:10.1016/j.epsl.2014.05.056.

Bashir, L., S. S. Gao, K. H. Liu, and K. Mickus (2011), Crustal structure and evolution beneath the Colorado Plateau and the southern Basin and Range Province: Results from receiver function and gravity studies, Geochem. Geophys. Geosyst., 12, 1525–2027, doi:10.1029/2011GC003563.

Bedle, H., and S. van der Lee (2009), S velocity variations beneath North America, J. Geophys. Res., 114(B7), doi:10.1029/2008JB005949.

Burdick, S., Vernon, F. L., Martynov, V., Eakins, J., Cox, T., Tytell, J., Mulder, T., White, M. C., Astiz, L., Pavlis, G. L. and R. D. van der Hilst (2017), Model Update May 2016: Upper-Mantle Heterogeneity beneath North America from Travel-Time Tomography with Global and USArray Data, Seismol. Res. Lett., 88(2A), 319-325, doi:10.1785/0220160186.

Calò, M., Bodin, T., and B. Romanowicz (2016), Layered structure in the upper mantle across North America from joint inversion of long and short period seismic data, Earth Planet. Sci. Lett., 499, 164-175, doi:10.1016/j.epsl.2016.05.054.

Chen, L. (2017), Layering of subcontinental lithospheric mantle, Science Bulletin, 62(14), 1030-1034, doi:10.1016/j.scib.2017.06.003.

Clarke, T. J. (1993), The complete ordered ray expansion-II. Multiphase body wave tomography, Geophys. J. Int., 115(2), 435-444. doi:10.1111/j.1365-246X.1993.tb01197.x.

Cox, P., Stubailo, I., and P. Davis (2016), Receiver function and geometric tomography along the Monterey microplate to test slab delamination or lithospheric drip models of the Isabella Anomaly, California, Bull. Seismol. Soc. Am., 106(1), 267-280, doi:10.1785/0120140339.

Dueker, K. G., and A. F. Sheehan (1997), Mantle discontinuity structure from midpoint stacks of converted P to S waves across the Yellowstone hotspot track. J. Geophys. Res., 102, 8313-8327, 1997.

Eaton, D. W., and A. Frederiksen (2007), Seismic evidence for convection driven motion of the North American plate, Nature, 446(7134), 428-431, doi:10.1038/nature05675.

Evanzia, D., Pulliam, J., Ainsworth, R., Gurrola, H., and K. Pratt (2014), Seismic Vp & Vs tomography of Texas & Oklahoma with a focus on the Gulf Coast margin, Earth Planet. Sci. Lett., 402, 148-156. Doi:10.1016/j.epsl.2013.12.027.

Faber, S., and G. Müller, G (1980), Sp phases from the transition zone between the upper and lower mantle, Bull. Seismol. Soc. Am., 70(2), 487-508.

Farra, V., and L. Vinnik (2000), Upper mantle stratification by P and S receiver functions, Geophys. J. Int., 141(3), 699-712. doi:10.1046/j.1365-246x.2000.00118.x.

Fischer, K. M., Ford, H. A., Abt, D. L., and C. A. Rychert (2010), The lithosphere-asthenosphere boundary, Annu. Rev. Earth Planet. Sci., 38, 551-575, doi:10.1146/annurev-earth-040809-152438.

Ford, H. A., Long, M. D., and E. A. Wirth (2016), Midlithospheric discontinuities and complex anisotropic layering in the mantle lithosphere beneath the Wyoming and Superior Provinces, J. Geophys. Res., 121(9), 6675-6697, doi:10.1002/2016JB012978.

Foster, K., Dueker, K., Schmandt, B., and H. Yuan (2014), A sharp cratonic lithosphere-asthenosphere boundary beneath the American Midwest and its relation to mantle flow, Earth Planet. Sci. Lett., 402, 82-89, doi:10.1016/j.epsl.2013.11.018.

Ganguly, J. (2005), Adiabatic decompression and melting of mantle rocks: An irreversible thermodynamic analysis, Geophys. Res. Lett., 32(6), doi:10.1029/2005GL022363.

Gao, S. S., and K. H. Liu (2014), Mantle transition zone discontinuities beneath the contiguous United States, J. Geophys. Res. Solid Earth, 119, 6452–6468, doi:10.1002/2014JB011253.

Green, D. H., Hibberson, W. O., Kovács, I., and A. Rosenthal (2010), Water and its influence on the lithosphere-asthenosphere boundary, Nature 467, 448-451, doi:10.1038/nature09369.

Griffin, W. L., O'Reilly, S. Y., Doyle, B. J., Pearson, N. J., Coopersmith, H., Kivi, K., Malkovets, V., and N. Pokhilenko (2004), Lithosphere mapping beneath the North American plate, Lithos, 77(1), 873-922, http://dx.doi.org/10.1016/j.lithos.2004.03.034.

Hansen, S. M., K. Dueker, and B. Schmandt (2015), Thermal classification of lithospheric discontinuities beneath USArray, Earth Planet. Sci. Lett., 431, 36–47, doi:10.1016/j.epsl.2015.09.009.

Hoffman, P. F. (1988), United plates of America, the birth of a craton: Early Proterozoic assembly and growth of Laurentia, Annu. Rev. Earth Planet. Sci., 16(1), 543-603, doi:10.1146/annurev.ea.16.050188.002551.

Hopper, E., and K. M. Fischer (2015), The meaning of midlithospheric discontinuities: A case study in the northern US craton, Geochem. Geophys. Geosys., 16(12), 4057-4083, doi:10.1002/2015GC006030.

Humphreys, E. D. (1995), Post-Laramide removal of the Farallon slab, western United States, Geology, 23(11), 987-990, doi:10.1130/00917613(1995)023¡0987:PLROTF¿2.3.CO;2.

Kennett, B. L. N., and E. R. Engdahl (1991), Traveltimes for global earthquake location and phase identification, Geophys. J. Int., 105, 429–465.

Kind, R., Yuan, X., and P. Kumar (2012), Seismic receiver functions and the lithosphere-asthenosphere boundary, Tectonophysics, 536, 25-43, doi:10.1016/j.tecto.2012.03.005.

Kumar, P., Kind, R., Yuan, X., and J. Mechie (2012), USArray receiver function images of the lithosphere-asthenosphere boundary, Seismol. Res. Lett., 83(3), 486-491, doi:10.1785/gssrl.83.3.486.

Langston, C. A. (1979), Structure under Mount Rainier, Washington, inferred from teleseismic body waves, J. Geophys. Res., 84(B9), 4749-4762, doi:10.1029/JB084iB09p04749.

Lekić, V., and K. M. Fischer (2014), Contrasting lithospheric signatures across the western United States revealed by Sp receiver functions, Earth Planet. Sci. Lett., 402, 90-98, doi:10.1016/j.epsl.2013.11.026.

Levander, A., and M. S. Miller (2012), Evolutionary aspects of lithosphere discontinuity structure in the western US, Geochem. Geophys. Geosys., 13(7), doi:10.1029/2012GC004056.

Li, X., Yuan, X., and R. Kind (2007), The lithosphere-asthenosphere boundary beneath the western United States, Geophys. J. Int., 170(2), 700-710, doi:10.1111/j.1365-246X.2007.03428.x.

Liu, K. H., and S. S. Gao (2010), Spatial variations of crustal characteristics beneath the Hoggar swell, Algeria, revealed by systematic analyses of receiver functions from a single seismic station, Geochem. Geophys. Geosyst., 11, Q08011, doi:10.1029/2010GC003091.

Liu, L., Gao, S. S., Liu, K. H., and K. Mickus (2017), Receiver function and gravity constraints on crustal structure and vertical movements of the Upper Mississippi Embayment and Ozark Uplift, J. Geophys. Res., 122, 4572-4583, doi:10.1002/2017JB014201.

Mareschal, J. C., and C. Jaupart (2004), Variations of surface heat flow and lithospheric thermal structure beneath the North American craton, Earth Planet. Sci. Lett., 223(1), 65-77, doi:10.1016/j.epsl.2004.04.002.

Mickus, K., Stern, R. J., Keller, G. R., and E. Y. Anthony (2009), Potential field evidence for a volcanic rifted margin along the Texas Gulf Coast, Geology, 37(5), 387-390, doi:10.1130/G25465A.1.

Mierdel, K., Keppler, H., Smyth, J. R., and F. Langenhorst (2007), Water solubility in aluminous orthopyroxene and the origin of Earth's asthenosphere, Science, 315(5810), 364-368, doi:10.1126/science.1135422.

Murphy, B. S., and G. D. Egbert (2017), Electrical conductivity structure of southeastern North America: Implications for lithospheric architecture and Appalachian topographic rejuvenation, Earth Planet. Sci. Lett., 462, 66-75, doi:10.1016/j.epsl.2017.01.009.

Reeves, Z., Lekić, V., Schmerr, N., Kohler, M., and D. Weeraratne (2015), Lithospheric structure across the California Continental Borderland from receiver functions, Geochem. Geophys. Geosyst., 16(1), 246-266, doi:10.1002/2014GC005617.

Rychert, C. A., Rondenay, S., and K. M. Fischer (2007), P-to-S and S-to-P imaging of a sharp lithosphere-asthenosphere boundary beneath eastern North America, J. Geophys. Res., 112(B8), doi:10.1029/2006JB004619.

Schaeffer, A. J., and S. Lebedev (2014), Imaging the North American continent using waveform inversion of global and USArray data. Earth Planet. Sci. Lett. 402, 26-41, doi:10.1016/j.epsl.2014.05.014.

Sheriff, R. E., and L. P. Geldart (1982), Exploration seismology. Volume 1: History, theory, and data acquisition. Cambridge University Press, Cambridge.

Thibault, Y., Edgar, A. D., and F. E. Lloyd (1992), Experimental investigation of melts from a carbonated phlogopite lherzolite: implications for metasomatism in the continental lithospheric mantle, Am. Mineral., 77, 784-794.

Walowski, K. J., Wallace, P. J., Clynne, M. A., Rasmussen, D. J., and D. Weis (2016), Slab melting and magma formation beneath the southern Cascade arc, Earth Planet. Sci. Lett., 446, 100-112, doi:10.1016/j.epsl.2016.03.044.

Yang, B. B., Gao, S. S., Liu, K. H., Elsheikh, A. A., Lemnifi, A. A., Refayee, H. A., and Y. Yu (2014), Seismic anisotropy and mantle flow beneath the northern Great Plains of North America, J. Geophys. Res., 119(3), 1971-1985, doi:10.1002/2013JB010561.

Yan, Z., and R. W. Clayton (2007), Regional mapping of the crustal structure in southern California from receiver functions, J. Geophys. Res., 112(B5), doi:10.1029/2006JB004622.

Yuan, H., and B. Romanowicz (2010), Lithospheric layering in the North American craton. Nature, 466(7310), 1063-1068, doi:10.1038/nature09332.

Zhu, L., and H. Kanamori (2000), Moho depth variation in southern California from teleseismic receiver functions, J. Geophys. Res., 105, 2969–2980, doi:10.1029/1999JB900322.

SECTION

2. CONCLUSIONS

In this research, we use all available broadband seismic data obtained from unprecedented spatial covered USArray Transportable Array (TA) and other seismic stations to analyze the negative-velocity discontinuities in the upper mantle in the contiguous United States and crustal thickness and Vp/Vs beneath the Upper Mississippi Embayment and Ozark Uplift. As a consequence of the analyses of these data sets, numerous significant findings are reportable.

1) A robust negative velocity discontinuity is pervasively detected in the contiguous U.S. in the depth range of 30-110 km in consecutive 2° circular bins using 284,121 S-to-P receiver functions that is unprecedented for the study area. Beneath the extended crust of the western U.S. and the Gulf Coastal Plain and the eastern U.S., similarities between the depth of the this discontinuity and depths of the LAB revealed by seismic tomography and xenolith studies suggests that it represents the sharp transitional layer between the cold lithosphere and partially melt asthenosphere. In contrast, beneath the stable cratonic region of the central U.S., this discontinuity is most likely the sharp upper boundary of a chemically distinct layer probably formed by metasomatism in the ancient lithosphere.

An intriguing anti-correlation between the depth of the negative velocity discontinuity and the amplitude of the Sp wave is revealed for the western U.S. One of the simplest explanations for this relationship is that the top-most layer of the asthenosphere experiences more volatile-induced melting beneath thinner lithosphere.

Uniform extension of the lithosphere in the Basin and Range Province and the Texas-Louisiana Gulf Coastal Plain can satisfactorily explain the observed thinning of the crust and the whole lithosphere. Finally, anomalously thin lithosphere and large stacking amplitudes observed beneath the northeastern U.S. may indicate erosion of the bottom of the lithosphere, probably by a passing mantle plume.

2) The first sedimentary-removal P-to-S receiver function (PRF) study, employing 49 stations beneath the Upper Mississippi Embayment (UME) and the Ozark Uplift, has been conducted. Observations of crustal properties measured using PRFs and gravity anomaly data confirm the existence of a mafic, high-density lower crustal layer beneath the UME, and reveal a high-density mafic upper crustal layer which is not commonly found beneath other continental rifts. The previously inferred dominantly Cretaceous age of the mafic intrusions found in the UME and the approximately 2 km rise of the area preceding the post-Cretaceous subsidence suggest a possible role of a passing mantle plume on the tectonic evolution of the UME. Intrusion of mantle material into the UME crust fractured by rifting during the Late Precambrian increased the bulk density of the crust, leading to renewed subsidence after the plume moved away from the area. The Ozark Uplift, in contrast, is characterized by normal crustal thickness and Vp/Vs measurements that are similar to those of midcontinent cratonic crust, suggesting that the plume did not penetrate the strong and thick lithosphere beneath the Ozark Uplift.

BIBLIOGRAPHY

Abt, D. L., Fischer, K. M., French, S. W., Ford, H. A., Yuan, H., and B. Romanowicz (2010), North American lithospheric discontinuity structure imaged by Ps and Sp receiver functions, J. Geophys. Res. 115(B9), doi:10.1029/2009JB006914.

Ainsworth, R., Pulliam, J., Gurrola, H., and D. Evanzia (2014), Sp receiver function imaging of a passive margin: Transect across Texas's Gulf Coastal Plain, Earth Planet, Sci. Lett., 402, 138-147, doi:10.1016/j.epsl.2014.05.056.

Ammon, C. J. (1991), The isolation of receiver effects from teleseismic P waveforms, Bull. Seismol. Soc. Am., 81, 2504–2510.

Bashir, L., S. S. Gao, K. H. Liu, and K. Mickus (2011), Crustal structure and evolution beneath the Colorado Plateau and the southern Basin and Range Province: Results from receiver function and gravity studies, Geochem. Geophys. Geosyst., 12, 1525–2027, doi:10.1029/2011GC003563.

Bedle, H., and S. van der Lee (2009), S velocity variations beneath North America, J. Geophys. Res., 114(B7), doi:10.1029/2008JB005949.

Benoit, M. H., M. D. Long, and S. D. King (2013), Anomalously thin transition zone and apparently isotropic upper mantle beneath Bermuda: Evidence for upwelling, Geochem. Geophys. Geosyst., 14, 4282–4291, doi:10.1002/ggge.20277.

Birt, C. S., P. K. H. Maguire, M. A. Khan, H. Thybo, G. R. Keller, and J. Patel (1997), The influence of pre-existing structures on the evolution of the southern Kenya Rift valley: Evidence from seismic and gravity studies, Tectonophysics, 278, 211–242.

Braile, L. W., W. J. Hinze, G. R. Keller, E. G. Lidiak, and J. L. Sexton (1986), Tectonic development of the New Madrid rift complex, Mississippi embayment, North America, Tectonophysics, 131, 1–21, doi:10.1016/0040-1951(86)90265-9.

Burdick, S., Vernon, F. L., Martynov, V., Eakins, J., Cox, T., Tytell, J., Mulder, T., White, M. C., Astiz, L., Pavlis, G. L. and R. D. van der Hilst (2017), Model Update May 2016: Upper-Mantle Heterogeneity beneath North America from Travel-Time Tomography with Global and USArray Data, Seismol. Res. Lett., 88(2A), 319-325, doi:10.1785/0220160186.

Calò, M., Bodin, T., and B. Romanowicz (2016), Layered structure in the upper mantle across North America from joint inversion of long and short period seismic data, Earth Planet. Sci. Lett., 499, 164-175, doi:10.1016/j.epsl.2016.05.054.

Catchings, R. D. (1999), Regional Vp, Vs, Vp/Vs, and Poisson's ratios across earthquake source zones from Memphis, Tennessee, to St. Louis, Missouri, Bull. Seismol. Soc. Am., 89, 1591–1605.

Chen, C., D. Zhao, and S. Wu (2014), Crust and upper mantle structure of the New Madrid Seismic Zone: Insight into intraplate earthquakes, Phys. Earth Planet. Inter., 230, 1–14, doi:10.1016/j.pepi.2014.01.016.

Chen, L. (2017), Layering of subcontinental lithospheric mantle, Science Bulletin, 62(14), 1030-1034, doi:10.1016/j.scib.2017.06.003.

Chiu, J. M., A. C. Johnston, and Y. T. Yang (1992), Imaging the active faults of the central New Madrid seismic zone using PANDA array data, Seismol. Res. Lett., 63, 375–393, doi:10.1785/gssrl.63.3.375.

Christensen, N. I. (1996), Poisson's ratio and crustal seismology, J. Geophys. Res., 101, 3139–3156, doi:10.1029/95JB03446.

Christensen, N. I., and W. D. Mooney (1995), Seismic velocity structure and composition of the continental crust: A global view, J. Geophys. Res., 100, 9761–9788, doi:10.1029/95JB00259.

Chulick, G. S., and W. D. Mooney (2002), Seismic structure of the crust and uppermost mantle of North America and adjacent oceanic basins: A synthesis, Bull. Seismol. Soc. Am., 92, 2478–2492, doi:10.1785/0120010188.

Clarke, T. J. (1993), The complete ordered ray expansion-II. Multiphase body wave tomography, Geophys. J. Int., 115(2), 435-444. doi:10.1111/j.1365-246X.1993.tb01197.x.

Cox, P., Stubailo, I., and P. Davis (2016), Receiver function and geometric tomography along the Monterey microplate to test slab delamination or lithospheric drip models of the Isabella Anomaly, California, Bull. Seismol. Soc. Am., 106(1), 267-280, doi:10.1785/0120140339.

Cox, R. T., and R. B. Van Arsdale (1997), Hotspot origin of the Mississippi embayment and its possible impact on contemporary seismicity, Eng. Geol., 46, 201–216, doi:10.1016/S0013-7952(97)00003-3.

Cox, R. T., and R. B. Van Arsdale (2002), The Mississippi Embayment, North America: A first order continental structure generated by the Cretaceous superplume mantle event, J. Geodyn., 34, 163–176, doi:10.1016/S0264-3707(02)00019-4.

Dart, R. L., and H. S. Swolfs (1998), Contour mapping of relic structures in the Precambrian basement of the Reelfoot rift, North American midcontinent, Tectonics, 17, 235–249.

DeRito, R. F., F. A. Cozzarelli, and D. S. Hodge (1983), Mechanism of subsidence of ancient cratonic rift basins, Tectonophysics, 94, 141–168, doi:10.1016/0040-1951(83)90014-8.

Dueker, K. G., and A. F. Sheehan (1997), Mantle discontinuity structure from midpoint stacks of converted P to S waves across the Yellowstone hotspot track. J. Geophys. Res., 102, 8313-8327, 1997.

Eaton, D. W., and A. Frederiksen (2007), Seismic evidence for convection driven motion of the North American plate, Nature, 446(7134), 428-431, doi:10.1038/nature05675.

England, R. W., and J. Ebbing (2012), Crustal structure of central Norway and Sweden from integrated modelling of teleseismic receiver functions and the gravity anomaly, Geophys. J. Int., 191, 1–11, doi:10.1111/j.1365-246X.2012.05607.x.

Ervin, C. P., and L. D. McGinnis (1975), Reelfoot rift: Reactivated precursor to the Mississippi embayment, Geol. Soc. Am. Bull., 86, 1287–1295, doi:10.1130/0016-7606(1975)862.0.CO;2.

Evanzia, D., Pulliam, J., Ainsworth, R., Gurrola, H., and K. Pratt (2014), Seismic Vp & Vs tomography of Texas & Oklahoma with a focus on the Gulf Coast margin, Earth Planet. Sci. Lett., 402, 148-156. Doi:10.1016/j.epsl.2013.12.027.

Faber, S., and G. Müller, G (1980), Sp phases from the transition zone between the upper and lower mantle, Bull. Seismol. Soc. Am., 70(2), 487-508.

Farra, V., and L. Vinnik (2000), Upper mantle stratification by P and S receiver functions, Geophys. J. Int., 141(3), 699-712. doi:10.1046/j.1365-246x.2000.00118.x.

Fischer, K. M., Ford, H. A., Abt, D. L., and C. A. Rychert (2010), The lithosphere-asthenosphere boundary, Annu. Rev. Earth Planet. Sci., 38, 551-575, doi:10.1146/annurev-earth-040809-152438.

Ford, H. A., Long, M. D., and E. A. Wirth (2016), Midlithospheric discontinuities and complex anisotropic layering in the mantle lithosphere beneath the Wyoming and Superior Provinces, J. Geophys. Res., 121(9), 6675-6697, doi:10.1002/2016JB012978.

Foster, K., Dueker, K., Schmandt, B., and H. Yuan (2014), A sharp cratonic lithosphere-asthenosphere boundary beneath the American Midwest and its relation to mantle flow, Earth Planet. Sci. Lett., 402, 82-89, doi:10.1016/j.epsl.2013.11.018.

Ganguly, J. (2005), Adiabatic decompression and melting of mantle rocks: An irreversible thermodynamic analysis, Geophys. Res. Lett., 32(6), doi:10.1029/2005GL022363.

Gao, S. S., and K. H. Liu (2014), Mantle transition zone discontinuities beneath the contiguous United States, J. Geophys. Res. Solid Earth, 119, 6452–6468, doi:10.1002/2014JB011253.

Green, D. H., Hibberson, W. O., Kovács, I., and A. Rosenthal (2010), Water and its influence on the lithosphere-asthenosphere boundary, Nature 467, 448-451, doi:10.1038/nature09369.

Griffin, W. L., O'Reilly, S. Y., Doyle, B. J., Pearson, N. J., Coopersmith, H., Kivi, K., Malkovets, V., and N. Pokhilenko (2004), Lithosphere mapping beneath the North American plate, Lithos, 77(1), 873-922, http://dx.doi.org/10.1016/j.lithos.2004.03.034.

Hansen, S. M., K. Dueker, and B. Schmandt (2015), Thermal classification of lithospheric discontinuities beneath USArray, Earth Planet. Sci. Lett., 431, 36–47, doi:10.1016/j.epsl.2015.09.009.

Hildenbrand, T. G. (1985), Rift structure of the northern Mississippi embayment from the analysis of gravity and magnetic data, J. Geophys. Res., 90, 12,607–12,622, doi:10.1029/JB090iB14p12607.

Hildenbrand, T. G., and J. D. Hendricks (1995), Geophysical setting of the Reelfoot rift and relations between rift structures and the New Madrid seismic zone, US Geol. Surv. E1538, U.S. Geol. Surv., Washington, D. C.

Hildenbrand, T. G., A. Griscom, W. R. Van Schmus, and W. D. Stuart (1996), Quantitative investigations of the Missouri gravity low: A possible expression of a large, Late Precambrian batholith intersecting the New Madrid seismic zone, J. Geophys. Res., 101, 21,921–21,942, doi:10.1029/96JB01908.

Hoffman, P. F. (1988), United plates of America, the birth of a craton: Early Proterozoic assembly and growth of Laurentia, Annu. Rev. Earth Planet. Sci., 16(1), 543-603, doi:10.1146/annurev.ea.16.050188.002551.

Hopper, E., and K. M. Fischer (2015), The meaning of midlithospheric discontinuities: A case study in the northern US craton, Geochem. Geophys. Geosys., 16(12), 4057-4083, doi:10.1002/2015GC006030.

Humphreys, E. D. (1995), Post-Laramide removal of the Farallon slab, western United States, Geology, 23(11), 987-990, doi:10.1130/00917613(1995)023¡0987:PLROTF¿2.3.CO;2.

Ives, B., K. Mickus, A. McCafferty, C. Seeger, and M. Starkey (2014), Analyzing the Paleozoic basement structure and lithologies of the northwest St. Francois Terrance, Missouri using gravity data to investigate possible mineral deposits of economic interest, Geol. Soc. Am. Abstr. Programs, 46, 308.

Kane, M. F., T. G. Hildenbrand, and J. D. Hendricks (1981), Model for the tectonic evolution of the Mississippi Embayment and its contemporary seismicity, Geology, 9, 563–568, doi:10.1130/0091-7613(1981).9.2.0.CO;2.

Keller, G. R. (2013), The Moho of North America: A brief review focused on recent studies, Tectonophysics, 609, 45–55, doi:10.1016/j.tecto.2013.07.031.

Keller, G. R., M. A. Khan, P. Morgan, R. F. Wendlandt, W. S. Baldridge, K. H. Olsen, C. Prodehl, and L. W. Braile (1991), A comparative study of the Rio Grande and Kenya rifts, Tectonophysics, 197, 355–371.

Keller, G. R., R. F. Wendlandt, and M. H. P. Bott (2006), West and central African rift system, Dev. Geotectonics, 25, 437–449.

Kennett, B. L. N., and E. R. Engdahl (1991), Traveltimes for global earthquake location and phase identification, Geophys. J. Int., 105, 429–465.

Kind, R., Yuan, X., and P. Kumar (2012), Seismic receiver functions and the lithosphere-asthenosphere boundary, Tectonophysics, 536, 25-43, doi:10.1016/j.tecto.2012.03.005.

Kumar, P., Kind, R., Yuan, X., and J. Mechie (2012), USArray receiver function images of the lithosphere-asthenosphere boundary, Seismol. Res. Lett., 83(3), 486-491, doi:10.1785/gssrl.83.3.486.

Langston, C. A. (1977), The effect of planar dipping structure on source and receiver responses for constant ray parameter, Bull. Seismol. Soc. Am., 67, 1029–1050.

Langston, C. A. (1979), Structure under Mount Rainier, Washington, inferred from teleseismic body waves, J. Geophys. Res., 84(B9), 4749-4762, doi:10.1029/JB084iB09p04749.

Larson, M., and K. Mickus (2013), Gravity and magnetic analysis of plutons, ring plutons and mafic bodies in the St. Francois Mountains, SE Missouri, Geol. Soc. Am. Abstr. Programs, 45, 2.

Lekić, V., and K. M. Fischer (2014), Contrasting lithospheric signatures across the western United States revealed by Sp receiver functions, Earth Planet. Sci. Lett., 402, 90-98, doi:10.1016/j.epsl.2013.11.026.

Levander, A., and M. S. Miller (2012), Evolutionary aspects of lithosphere discontinuity structure in the western US, Geochem. Geophys. Geosys., 13(7), doi:10.1029/2012GC004056.

Li, X., Yuan, X., and R. Kind (2007), The lithosphere-asthenosphere boundary beneath the western United States, Geophys. J. Int., 170(2), 700-710, doi:10.1111/j.1365-246X.2007.03428.x.

Liang, C., and C. A. Langston (2009), Three-dimensional crustal structure of eastern North America extracted from ambient noise, J. Geophys. Res., 114, B03310, doi:10.1029/2008JB005919.

Liu, K. H., and S. S. Gao (2010), Spatial variations of crustal characteristics beneath the Hoggar swell, Algeria, revealed by systematic analyses of receiver functions from a single seismic station, Geochem. Geophys. Geosyst., 11, Q08011, doi:10.1029/2010GC003091.

Liu, L., Gao, S. S., Liu, K. H., and K. Mickus (2017), Receiver function and gravity constraints on crustal structure and vertical movements of the Upper Mississippi Embayment and Ozark Uplift, J. Geophys. Res., 122, 4572-4583, doi:10.1002/2017JB014201.

Logatchev, N. A., and N. A. Florensov (1978), The Baikal system of rift valleys, Tectonophysics, 45, 1–13.

Mareschal, J. C., and C. Jaupart (2004), Variations of surface heat flow and lithospheric thermal structure beneath the North American craton, Earth Planet. Sci. Lett., 223(1), 65-77, doi:10.1016/j.epsl.2004.04.002.

McCamy, K., and R. P. Meyer (1966), Crustal results of fixed multiple shots in the Mississippi embayment, in The Earth Beneath the Continents, edited by J. S. Steinhart and T. J. Smith, pp. 370–381, AGU, Washington, D. C., doi:10.1029/GM010p0370.

McGlannan, A. J., and H. Gilbert (2016), Crustal signatures of the tectonic development of the North American midcontinent, Phys. Earth Planet. Inter., 433, 339–349, doi:10.1016/j.epsl.2015.10.048.

Mickus, K., Stern, R. J., Keller, G. R., and E. Y. Anthony (2009), Potential field evidence for a volcanic rifted margin along the Texas Gulf Coast, Geology, 37(5), 387-390.

Mierdel, K., Keppler, H., Smyth, J. R., and F. Langenhorst (2007), Water solubility in aluminous orthopyroxene and the origin of Earth's asthenosphere, Science, 315(5810), 364-368, doi:10.1126/science.1135422.

Mooney, W. D., M. C. Andrews, A. Ginzburg, D. A. Peters, and R. M. Hamilton (1983), Crustal structure of the northern Mississippi embayment and a comparison with other continental rift zones, Tectonophysics, 94, 327–348.

Morelli, C. (1976), Modern standards for gravity surveys, Geophysics, 41, 1051, doi:10.1190/1.1440661. Nair, S. K., S. S. Gao, K. H. Liu, and P. G. Silver (2006), Southern African crustal evolution and composition: Constraints from receiver function studies, J. Geophys. Res., 111, B02304, doi:10.1029/2005JB003802.

Murphy, B. S., and G. D. Egbert (2017), Electrical conductivity structure of southeastern North America: Implications for lithospheric architecture and Appalachian topographic rejuvenation, Earth Planet. Sci. Lett., 462, 66-75, doi:10.1016/j.epsl.2017.01.009.

Pollitz, F. F., and W. D. Mooney (2014), Seismic structure of the central US crust and shallow upper mantle: Uniqueness of the Reelfoot Rift, Earth Planet. Sci. Lett., 402, 157–166, doi:10.1016/j.epsl.2013.05.042.

Ramírez-Guzmán, L., O. S. Boyd, S. Hartzell, and R. A. Williams (2012), Seismic velocity model of the central United States (version 1): Description and simulation of the 18 April 2008 Mt. Carmel, Illinois, earthquake, Bull. Seismol. Soc. Am., 102, 2622–2645, doi:10.1785/0120110303.

Reed, C. A., S. Almadani, S. S. Gao, A. A. Elsheikh, S. Cherie, M. G. Abdelsalam, A. K. Thurmond, and K. H. Liu (2014), Receiver function constraints on crustal seismic velocities and partial melting beneath the Red Sea rift and adjacent regions, Afar Depression, J. Geophys. Res. Solid Earth, 119, 2138–2152, doi:10.1002/2013JB010719.

Reeves, Z., Lekić, V., Schmerr, N., Kohler, M., and D. Weeraratne (2015), Lithospheric structure across the California Continental Borderland from receiver functions, Geochem. Geophys. Geosyst., 16(1), 246-266, doi:10.1002/2014GC005617.

Rychert, C. A., Rondenay, S., and K. M. Fischer (2007), P-to-S and S-to-P imaging of a sharp lithosphere-asthenosphere boundary beneath eastern North America, J. Geophys. Res., 112(B8), doi:10.1029/2006JB004619.

Schaeffer, A. J., and S. Lebedev (2014), Imaging the North American continent using waveform inversion of global and USArray data. Earth Planet. Sci. Lett. 402, 26-41, doi:10.1016/j.epsl.2014.05.014.

Schiffer, C., N. Balling, J. Ebbing, B. H. Jacobsen, and S. B. Nielsen (2016), Geophysical-petrological modelling of the East Greenland Caledonides—Isostatic support from crust and upper mantle, Tectonophysics, 692, 44–57, doi:10.1016/j.tecto.2016.06.023.

Schwalb, H. R. (1969), Paleozoic geology of the Jackson Purchase region, Kentucky: Kentucky Geol. Surv. Rep. of Invest., 10, 40.

Sheriff, R. E., and L. P. Geldart (1982), Exploration seismology. Volume 1: History, theory, and data acquisition. Cambridge University Press, Cambridge.

Stewart, S. W. (1968), Crustal structure in Missouri by seismic-refraction methods, Bull. Seismol. Soc. Am., 58, 291–323.

Thibault, Y., Edgar, A. D., and F. E. Lloyd (1992), Experimental investigation of melts from a carbonated phlogopite lherzolite: implications for metasomatism in the continental lithospheric mantle, Am. Mineral., 77, 784-794.

Thomas, W. A. (1991), The Appalachian-Ouachita rifted margin of southeastern North America, Geol. Soc. Am. Bull., 103, 415–431, doi:10.1130/0016-7606(1991)1032.3.CO;2.

Thybo, H., and I. M. Artemieva (2013), Moho and magmatic underplating in continental lithosphere, Tectonophysics, 609, 605–619.

Thybo, H., and C. A. Nielsen (2009), Magma-compensated crustal thinning in continental rift zones, Nature, 457, 873–876, doi:10.1038/nature07688.

Van Arsdale, R. B., and R. T. Cox (2007), The Mississippi's curious origins, Sci. Am., 296, 76–82.

Van Schmus, W. R. (1992), Tectonic setting of the midcontinent rift system, Tectonophysics, 213, 1–15, doi:10.1016/0040-1951(92)90247-4.

Walowski, K. J., Wallace, P. J., Clynne, M. A., Rasmussen, D. J., and D. Weis (2016), Slab melting and magma formation beneath the southern Cascade arc, Earth Planet. Sci. Lett., 446, 100-112, doi:10.1016/j.epsl.2016.03.044.

Watanabe, T. (1993), Effects of water and melt on seismic velocities and their application to characterization of seismic reflectors, Geophys. Res. Lett., 20, 2933–2936.

Wernicke, B., and J. K. Snow (1998), Cenozoic tectonism in the central Basin and Range: Motion of the Sierran-Great Valley block, Int. Geol. Rev., 40(5), 403-410, doi:10.1080/00206819809465217.

Wessel, P., and W. H. Smith (1991), Free software helps map and display data, Eos Trans. AGU, 72, 441–446.

Whitmeyer, S. J., and K. E. Karlstrom (2007), Tectonic model for the Proterozoic growth of North America, Geosphere, 3, 220–259, doi:10.1130/GES00055.1.

Wirth, E. A., and M. D. Long (2014), A contrast in anisotropy across mid-lithospheric discontinuities beneath the central United States-a relic of craton formation, Geology, 42(10), 851-854, doi:10.1130/G35804.1.

Yang, B. B., Gao, S. S., Liu, K. H., Elsheikh, A. A., Lemnifi, A. A., Refayee, H. A., and Y. Yu (2014), Seismic anisotropy and mantle flow beneath the northern Great Plains of North America, J. Geophys. Res., 119(3), 1971-1985.

Yan, Z., and R. W. Clayton (2007), Regional mapping of the crustal structure in southern California from receiver functions, J. Geophys. Res., 112(B5).

Yuan, H., and B. Romanowicz (2010), Lithospheric layering in the North American craton. Nature, 466(7310), 1063-1068, doi:10.1038/nature09332.

Yu, Y., J. Song, K. H. Liu, and S. S. Gao (2015a), Determining crustal structure beneath seismic stations overlying a low-velocity sedimentary layer using receiver functions, J. Geophys. Res. Solid Earth, 120, 3208–3218, doi:10.1002/2014JB011610.

Yu, Y., K. H. Liu, C. A. Reed, M. Moidaki, K. Mickus, E. A. Atekwana, and S. S. Gao (2015b), A joint receiver function and gravity study of crustal structure beneath the incipient Okavango Rift, Botswana, Geophys. Res. Lett., 42, 8398–8405.

Zelt, B. C., and R. M. Ellis (1999), Receiver-function studies in the Trans-Hudson orogen, Saskatchewan, Can. J. Earth Sci., 36, 585–603.

Zhu, L., and H. Kanamori (2000), Moho depth variation in southern California from teleseismic receiver functions, J. Geophys. Res., 105, 2969–2980, doi:10.1029/1999JB900322.

VITA

Lin Liu was born in the city of Yantai, China. She studied exploration technology and engineering at Ocean University of China and earned her Bachelor's degree in June 2013. She joined the Geology and Geophysics program at Missouri University of Science and Technology to pursue her Ph.D. degree in geophysics in August, 2013.

During her graduate studies, she was actively involved in various academic activities. She was an active member in the American Geophysical Union (AGU), Society of Exploration Geophysics (SEG), American Association of Petroleum Geologist (AAPG), and Geologic Society of America (GSA). She served as the vice president of the Missouri S&T chapter in 2015 and 2016. She presented her research works at the AGU annual meeting in 2014, 2015, 2016, and 2017. Her research focuses on the structure and dynamics of the Earth's crust and mantle using the methods of shear wave splitting and receiver function. She has single-handed written the suite of complicated programs to calculate and stack S-to-P receiver functions. She was offered the Outstanding Teaching Assistant Award in 2016 and Outstanding Graduate Scholar Award in 2017 in the whole Geology and Geophysics program. She was also received a 4-year scholarship from the China Scholarship Council.

In July 2018 she received her PhD degree in Geology and Geophysics from Missouri University of Science and Technology.